

CD-GraB: Coordinating Distributed Example Orders for Provably Accelerated Training

A. Feder Cooper*, Wentao Guo*, Khiem Pham*,
Tiancheng Yuan, Charlie F. Ruan, Yucheng Lu, Christopher De Sa

Cornell University
{afc78, wg247, dkp45, ty373, cfr54, yl2967, cmd353}@cornell.edu

June 18, 2024

Abstract

Recent research on online Gradient Balancing (GraB) has revealed that there exist permutation-based example orderings that are guaranteed to outperform random reshuffling (RR). Whereas RR arbitrarily permutes training examples, GraB leverages stale gradients from prior epochs to order examples — achieving a provably faster convergence rate than RR. However, GraB is limited by design: While it demonstrates an impressive ability to scale-up training on *centralized* data, it does not naturally extend to modern *distributed* ML workloads. We therefore propose *Coordinated Distributed GraB* (CD-GraB), which uses insights from prior work on kernel thinning to translate the benefits of provably faster permutation-based example ordering to distributed settings. With negligible overhead, CD-GraB exhibits a linear speedup in convergence rate over centralized GraB and outperforms baselines empirically, including distributed RR, on a variety of benchmark tasks.

1 Introduction

Random reshuffling, which samples training data examples without replacement, has become the *de facto* example ordering method in modern deep learning libraries [34], given that it tends to accelerate optimizer convergence in practice. However, some recent theoretical work has identified cases in which random reshuffling can lead to data orderings that have a poor effect on convergence [8, 36, 49]. This has encouraged a line of research to investigate if there exist provably better permutation-based orderings that afford greater scalability in training [22, 24, 31]. Notably, Lu et al. [24] connect permuted-order SGD to the *herding problem* [16], and proposes the herding-based online Gradient Balancing algorithm (GraB), which converges provably faster than random reshuffling, and does so with little memory or computational overhead. In fact, in follow-on work, Cha et al. [6] prove that GraB is optimal: In theory, GraB is the fastest possible permutation-based example ordering algorithm.

While these results are very exciting, suggesting that GraB should unseat random reshuffling as the example ordering method-of-choice, they only hold with respect to a *single* machine. GraB is optimal in settings with *centralized* data, but does not naturally translate to problems of modern ML scale, which demand that training workloads be distributed across *multiple parallel* workers that each only have access to a subset of the training data. This drawback raises an important question:

*Can we simultaneously achieve the scalability benefits of distributed training
and provably faster permutation-based example ordering — both in theory and in practice?*

In this work, we show that it is indeed possible to attain these twin objectives. To do so, we put forward the online **C**oordinated **D**istributed **G**radient **B**alance algorithm (CD-GraB), which leverages insights from kernel thinning to elevate the herding framework of centralized GraB (GraB) to the parallel setting. Felicitously, as a side effect, this choice of formulation brings about positive practical performance benefits (that can also

*Equal contribution; ordered alphabetically.

improve the empirical behavior of centralized GraB). Using the exact same assumptions as the original GraB paper, **we show analytically that coordinating example orders across parallel workers leads a linear speedup in convergence rate.** For T epochs and m parallel workers, each with access to n examples, CD-GraB’s convergence rate is $\tilde{O}((mnT)^{-2/3})$ on smooth, non-convex objectives and $\tilde{O}((mnT)^{-2})$ under the Polyak-Łojasiewicz (P.L.) condition.¹

We run a series of experiments to verify these improvements in practice, implementing CD-GraB on a single node that distributes computation across multiple GPUs. We also run an ablation study in order to disentangle the benefits of parallelism from the positive side effects of using kernel thinning to formulate the CD-GraB algorithm. Similar to how centralized GraB demonstrates improves generalization over centralized random reshuffling (RR), we observe that CD-GraB exhibits improved generalization over distributed random reshuffling (D-RR). Altogether, the success of our work suggests a new distributed training paradigm to explore in future work, which we call the *Order Server* (Section 6). In summary, we:

- Propose the online **C**oordinated **D**istributed **G**radient **B**alancing (CD-GraB) algorithm, which enables provably accelerated training in the parallel setting (Section 3);
- Prove that the convergence rate for CD-GraB exhibits a linear speedup over GraB, using the exact same assumptions as the original GraB paper (Section 4);
- Produce extensive empirical validation of CD-GraB’s improved scalability on a variety of tasks in deep learning and large-scale logistic regression (Section 5).

2 Preliminaries and Related Work

In this section, we discuss the preliminaries and prior scholarship on permutation-based example ordering, with particular attention paid to the centralized online Gradient Balancing Algorithm (GraB) [24]. This lays the groundwork for how our coordinated distributed GraB algorithm (Section 3) imparts the efficiency guarantees of GraB to the parallelized regime (Section 4).

Ordering data examples during training. Training a model can be formulated as minimizing a differentiable loss function $f : \mathbb{R}^d \rightarrow \mathbb{R}$ over N data examples. The goal of this minimization is to obtain the target model weights $\mathbf{w}^* = \arg \min_{\mathbf{w}} f(\mathbf{w})$, where $f(\mathbf{w}) = \frac{1}{N} \sum_{j=1}^N f(\mathbf{w}; j)$, where $f(\mathbf{w}; j)$ denotes the loss incurred on the j -th example. A typical training process is to iteratively update the model parameters \mathbf{w} by scanning over the N data examples repeatedly, with t -th scan (or epoch) following

$$\mathbf{w}_t^{j+1} = \mathbf{w}_t^j - \alpha \nabla f(\mathbf{w}_t^j; \pi_t(j)), \quad \forall j \in [N], \quad (1)$$

where α denotes the learning rate, and $\pi_t : [N] \rightarrow [N]$ denotes a permutation ordering² adopted in the t -th epoch from which the examples are chosen to compute gradients, \mathbf{w}_t^1 denotes the initial model weights for the t -th epoch, and \mathbf{w}_t^j denotes the model weights after $j - 1$ gradient updates in the t -th epoch.

The choice of ordering π can have a significant effect on optimizer performance. Two popular methods, which can demonstrate convergence speedups in practice, are random reshuffling (RR) [46], for which the permutations are random and differ over epochs, and Shuffle Once (SO) [4, 13], for which a random permutation is computed once and remains fixed for all epochs. Recht and Ré [37] conducted the first theoretical investigation of RR, while subsequent works like Yun et al. [49] and De Sa [8] have given counterexamples in which RR leads to poor orderings. Altogether, many studies indicate that RR and SO only provide efficiency benefits under certain conditions [14, 15, 30].

These limitations of RR and SO have motivated research to identify permutations that outperform random ones. Rajput et al. [36] introduce a RR variant, which achieves improved convergence for quadratics by reversing the ordering every other epoch. Other, non-RR-based methods leverage the relationship between correlations among adjacently selected examples and convergence. Lu et al. [22] prove that faster convergence is possible for SGD, when the averages of consecutive stochastic gradients converge faster to the full gradient. Based on this result, Lu et al. [24] propose the centralized online Gradient Balancing algorithm (GraB), which outperforms RR, and upon which we base this work.

¹In this paper, we use \tilde{O} by convention to hide logarithmic factors in the problem parameters.

²While without-replacement orderings are most common in large-scale learning [5], ordering strategies need not be permutations, e.g., with-replacement sampling [23, 32, 39] and curriculum learning [12, 27, 41].

2.1 GraB: Optimal, online, permutation-based example ordering for centralized ML

GraB is a permutation-based ordering algorithm that identifies provably better-than-random orderings *in centralized settings*. GraB finds such orderings by leveraging information in stale stochastic gradients from previous epochs to guide example ordering in the next epoch. More formally, for smooth, non-convex objectives, Lu et al. [24] prove that any permutation π^* that guarantees

$$\max_{k \in [N]} \left\| \sum_{j=1}^k \nabla f(\mathbf{w}; \pi^*(j)) - \nabla f(\mathbf{w}) \right\|_{\infty} = \tilde{O}(1) \quad (\nabla f(\mathbf{w}) \text{ is the average gradient}), \quad (2)$$

will yield a convergence rate of $\tilde{O}((NT)^{-2/3})$ (for epochs T), which is superior to the $O(N^{-1/3}T^{-2/3})$ convergence rate of random reshuffling [30].

GraB’s connection to herding and balancing. To find such a permutation π^* , Lu et al. [24] connect (2) to the *herding problem* and vector *balancing* [16, 45]. **Understanding why GraB does not naturally extend to the distributed setting — and our main contributions in Sections 3 and 4 — requires some additional details on the fundamentals of herding:**

Given N vectors³ $\{\mathbf{z}_j\}_{j=1}^N$ ($\mathbf{z}_j \in \mathbb{R}^d$), $\|\mathbf{z}_j\|_2 \leq 1$ ($\forall j$), herding identifies a permutation π^* such that

$$\max_{k \in [N]} \left\| \sum_{j=1}^k (\mathbf{z}_{\pi^*(j)} - \bar{\mathbf{z}}) \right\|_{\infty} = \tilde{O}(1), \quad \text{where } \bar{\mathbf{z}} = \frac{1}{N} \sum_{j=1}^N \mathbf{z}_j. \quad (3)$$

It is clear that (3) generalizes (2), which is a specific case of herding in an optimization setting.

Harvey and Samadi [16] solve (3) with a method called *balancing*. Balancing uses a *signed* version of the herding problem to optimize any given permutation π to reduce the bound in (3). That is, balancing formulates the signed herding problem

$$\max_{k \in [N]} \left\| \sum_{j=1}^k s_{\pi(j)} (\mathbf{z}_{\pi(j)} - \bar{\mathbf{z}}) \right\|_{\infty}, \quad \text{where } \{s_j\}_{j=1}^N \in \{+1, -1\}. \quad (4)$$

Given a group of such signs $\{s_j\}_{j=1}^N$ and an arbitrary π , Harvey and Samadi [16] prove that Algorithm 1 produces a new permutation π' such that

$$\max_{k \in [N]} \left\| \sum_{j=1}^k (\mathbf{z}_{\pi'(j)} - \bar{\mathbf{z}}) \right\|_{\infty} \leq \frac{1}{2} \max_{k \in [N]} \left\| \sum_{j=1}^k s_{\pi(j)} (\mathbf{z}_{\pi(j)} - \bar{\mathbf{z}}) \right\|_{\infty} + \frac{1}{2} \max_{k \in [N]} \left\| \sum_{j=1}^k (\mathbf{z}_{\pi(j)} - \bar{\mathbf{z}}) \right\|_{\infty}.$$

This says that, with new permutation π' , the objective of (3) now approaches the bound of (4). Importantly, recent advances show that it is quite cheap to find a group of signs, such that (4) is on the order of $\tilde{O}(1)$ (e.g., Alweiss et al. [2], in Algorithm 2). We are therefore able to call Algorithm 1 repeatedly, which will eventually obtain the π^* that solves the herding objective in (3).

GraB’s application to herding to gradient balancing. Lu et al. [24] apply this framework of herding and balancing to develop GraB — to minimize (2). The main challenge for the success of this approach is to find the right gradients \mathbf{z}_j in the optimization context of (2). Notably, the herding and balancing framework requires the vector mean $\bar{\mathbf{z}}$ in advance. To satisfy this requirement, GraB “centers” the gradient vectors using a *stale mean*. That is, GraB runs the herding algorithm on vectors that are defined as

$$\mathbf{z}_j = \nabla f(\mathbf{w}_t^j; \pi_t(j)) - \frac{1}{N} \sum_{p=1}^N \nabla f(\mathbf{w}_{t-1}^p; \pi_{t-1}(p)), \quad (5)$$

³Herding does not have an optimization context. Here, N does *not* refer to the number of data examples used in training (1); rather, $N \in \mathbb{Z}^+$ describes the size of a set of arbitrary vectors. We slightly abuse notation because in Section 3 we execute the herding subroutine on exactly N gradients, which happen to equal the number of N examples.

Algorithm 1 Reordering Vectors based on Balanced Signs [Harvey and Samadi [16]]

input: a group of signs $\{s_j\}_{j=1}^N$, initial order π
initialize: two order-sensitive lists $L_{\text{pos}} \leftarrow []$, $L_{\text{neg}} \leftarrow []$.
for $j = 1 \dots N$ **do**
 $L_{\text{pos}}.\text{append}(\pi(j))$ **if** s_j is +1 **else** $L_{\text{neg}}.\text{append}(\pi(j))$.
end for
return: new order $\pi' := \text{concat}(L_{\text{pos}}, \text{reverse}(L_{\text{neg}}))$.

where \mathbf{w}_t^p denotes the model weights after $p - 1$ updates in the t -th epoch, and π_t denotes the permutation adopted in the t -th epoch. Lu et al. [24] prove that this definition of \mathbf{z}_j preserves the benefits of balancing with negligible noise or overhead. The only overhead comes from storing the running average of the gradients in epoch $t - 1$ to “center” the gradients in the subsequent epoch t .

With this approach, Lu et al. [24] prove that GraB is more efficient than RR. Better still, Cha et al. [6] demonstrate that GraB is in fact the *optimal* permutation-based ordering method: It is not possible to produce a permutation-based ordering in the centralized setting that achieves a faster convergence rate. **Despite GraB’s clear benefits over RR, no present work has attempted to investigate its applicability to the parallel setting.** While some work has studied distributed RR (D-RR) [18, 26, 38, 48], it remains an open question if GraB’s efficiency benefits can be conferred to the modern-scale distributed ML setup.

3 CD-GraB: A Provably Efficient Ordering Algorithm for Distributed Training

Our main contribution is to elevate GraB to the parallel regime, so that distributed training can enjoy the efficiency benefits of provably better example ordering. Based on the preliminaries we can now explain why this is not a straightforward task: **While GraB achieves the optimal convergence rate on centralized data, it does not naturally translate to a distributed setting** (Section 3.1). Our key insights for resolving these problems are to reformulate the herding framework in Lu et al. [24] to work in parallel, and to leverage kernel thinning [3, 10, 11] to derive the *online* PairBalance algorithm, which solves the parallel herding objective (Section 3.2). Lastly, we present the full-stack CD-GraB algorithm that makes our solution work in practice (Section 3.3). The server implements online PairBalance, which coordinates gradient information from the distributed workers in training epoch t in order to determine a provably efficient example order for the next epoch $t + 1$ (Section 4).

3.1 Issues with GraB in the distributed setting

To clarify the issues with implementing GraB in the distributed setting, we first need to define the distributed training setup more precisely. We consider the standard data-parallel training regime with m parallel workers, where each worker keeps a copy of the model weights $\mathbf{w} \in \mathbb{R}^d$ and maintains $n = N/m$ local data examples.⁴ As in many data-parallel training applications,⁵ such as geo-distributed model training [47], we assume *the data examples cannot be shared or moved across workers*. More formally, this setup can be expressed as

$$\min_{\mathbf{w} \in \mathbb{R}^d} \left[f(\mathbf{w}) = \frac{1}{m} \sum_{i=1}^m f^i(\mathbf{w}) \right] \quad \text{with} \quad f^i(\mathbf{w}) = \frac{1}{n} \sum_{j=1}^n f^i(\mathbf{w}; j), \quad (6)$$

where $f^i(\mathbf{w}; j) : \mathbb{R}^d \rightarrow \mathbb{R}$, $j \in [n]$, denotes the loss incurred on the j -th example on the i -th worker for model weights \mathbf{w} . We can now consider running (1) using this setup, for which each worker scans over their n local data examples using (potentially) different permutations. We denote $\pi_{t,i} : [n] \rightarrow [n]$ as the permutation-based ordering adopted on the i -th worker in the t -th training epoch. The update to the model can then be summarized as

⁴Without loss of generality, we assume that $N \bmod m = 0$ and that $n \bmod 2 = 0$.

⁵One such popular paradigm is federated learning, in which edge devices collaboratively train a model via small local updates [28, e.g.]. Federated learning typically involves highly imbalanced loads, partial user participation, and privacy-preserving mechanisms. These characteristics are orthogonal to what we consider here for example order. For CD-GraB, we focus on the regime of using parallelism to accelerate training, e.g., in a data center context.

$$\mathbf{w}_t^{j+1} = \mathbf{w}_t^j - \frac{\alpha}{m} \sum_{i=1}^m \nabla f^i(\mathbf{w}_t^j; \pi_{t,i}(j)), \quad \forall j \in [n]. \quad (7)$$

That is, in epoch t , each worker i selects their respective, local j -th example according to $\{\pi_{t,i}\}_{i=1}^n$ in order to compute stochastic gradients (Appendix).

Following this setup, Algorithm 1 no longer guarantees the $\tilde{O}(1)$ bound to the herding problem (3), a bound that is valid only when *all* data examples can be permuted *freely* [16]. This constraint is fine for centralized GraB, but, in distributed training, workers only have access to a *subset* of examples. Distributed training requires that *worker-specific permutations only involve the examples in their respective local subsets*. Further, recall that GraB uses stale means to center gradients (5) in order to solve the herding objective. This, too, causes problems in distributed training. In practice, it is typical to employ larger learning rates α for greater scalability [40]; larger α increases the discrepancy between averaged gradients in adjacent epochs, which, in turn, would make GraB’s use of stale means unreliable.

3.2 Our efficient solution: Parallel herding and pair balancing

To address the limitations presented in the prior section, which preclude the direct application of GraB to distributed training, we will need to **1) reformulate the herding problem to fit the parallel setting and 2) redesign how to do gradient balancing**, such that it both solves our new herding formulation and allows for reliability with higher learning rates. In this section, we present our solution to both these problems; we introduce the *parallel herding* problem and the online PairBalance subroutine that solves it.

Parallel Herding. To extend herding to the parallel setting, consider the following setup: There are m workers, which each have local access to n vectors individually. Let $\mathbf{z}_{i,j} \in \mathbb{R}^d$ denote the vector indexed by j on the i -th worker. Assuming $\|\mathbf{z}_{i,j}\|_2 \leq 1$ ($\forall i \in [m], \forall j \in [n]$), the goal of parallel herding is to find m permutations, $\pi_1, \pi_2 \dots \pi_m$ where $\pi_i : [n] \rightarrow [n]$ ($\forall i \in [m]$), so as to minimize:

$$\max_{k \in [n]} \left\| \sum_{j=1}^k \sum_{i=1}^m (\mathbf{z}_{i,\pi_i(j)} - \bar{\mathbf{z}}) \right\|_{\infty}, \quad \text{with} \quad \bar{\mathbf{z}} = \frac{1}{mn} \sum_{i=1}^m \sum_{j=1}^n \mathbf{z}_{i,j}. \quad (8)$$

When directly comparing (8) with (3), it is clear that parallel herding differs in two notable ways from the original herding problem. First, each permutation $\pi_i : [n] \rightarrow [n]$ ($\forall i \in [m]$) only decides the ordering of vectors that are associated with worker i . Second, the prefix sum taken in the objective norm is accumulated over all the workers (the inner sum from $i = 1 \dots m$). This formulation naturally captures the setting in a distributed environment: **Workers need to decide permutations collaboratively, and the worker-specific vectors are processed simultaneously rather than sequentially.**

Given that this formulation fits the distributed setting, we next need to show that parallel herding does in fact address the limitations posed by centralized GraB: That it is possible to recover the $\tilde{O}(1)$ original herding bound and that we can solve the issue of unreliable stale gradients (Section 3.1). The solution that we present in the remainder of this section is a new vector balancing subroutine: online PairBalance. To give an intuition, as its name suggests, online PairBalance leverages insights from kernel thinning to *balance* vector differences over vector *pairs*. This eliminates the need to perform vector centering, and thus solves the stale mean problem, and also minimizes the parallel herding objective to be $\tilde{O}(1)$.

Using kernel thinning to solve parallel herding. We call our solution to the parallel herding objective *pair balancing*, which we derive based on key insights from recent research on *kernel thinning* [3, 10, 11]. In particular, Dwivedi and Mackey [10] show that it is possible to solve the herding objective in $\tilde{O}(1)$ **by only examining differences on pairs of examples**. They derive an algorithm that generalizes Alweiss et al. [2, subroutine in Algorithm 2], which solves herding in $\tilde{O}(1)$ (Section 2), and does so by operating only on pair differences.⁶ This comes with a very useful property: It eliminates the requirement of knowing the maximum

⁶[10] minimizes the maximum mean discrepancy (MMD) between a selected coreset and an empirical distribution, and develops a new self-balancing Hilbert walk on differences of *pairs of examples* in order to select exactly half of the dataset points. They solve coreset selection by iteratively halving the input vector sequence into balanced coresets, then selecting and refining a candidate coreset to minimize MMD with the input sequence.

Algorithm 2 PairBalance

▷ The inputs, outputs and subroutine for this algorithm are order-sensitive

input: current running sum \mathbf{r} , paired vectors $\mathbf{z}_1, \mathbf{z}_2$

compute: $s, \mathbf{r} \leftarrow \text{RandomizedBalance}(\mathbf{r}, \mathbf{z}_1 - \mathbf{z}_2)$

return: s (sign for \mathbf{z}_1),
 $-s$ (sign for \mathbf{z}_2),
 \mathbf{r} (updated running sum)

▷ From Alweiss et al. [2]

define subroutine: RandomizedBalance(\mathbf{r}, c)

compute: $p \leftarrow \frac{1 - \langle \mathbf{r}, c \rangle}{2}$

compute: $s \leftarrow +1$ with probability p ;
 $s \leftarrow -1$ with probability $1 - p$

update: $\mathbf{r} \leftarrow \mathbf{r} + sc$

return: s, \mathbf{r}

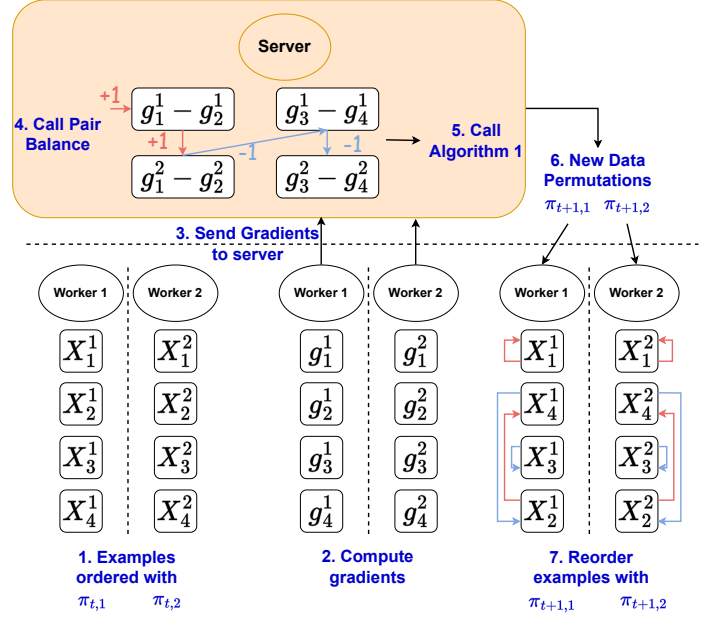


Figure 1: **Left:** The PairBalance algorithm, which the server runs online. **Right:** CD-GraB running on one server (top) and two workers (bottom). The workers do not share data examples.

vector norm ahead of time and centering the vectors (i.e., making all the vectors sum to zero) in order to solve the herding problem. This is the key to solving the parallel herding objective (8) in $\tilde{O}(1)$, and elevating the benefits of GraB to a distributed setting.

Following Dwivedi and Mackey [10], we will balance over paired vectors, and will do so in an *online* fashion (Section 3.3). This eliminates GraB’s requirement of using a stale mean to center gradient vectors (Section 2.1), but still minimizes the parallel herding objective to $\tilde{O}(1)$! We defer proving this to Section 4, and here describe our concrete algorithm. Online PairBalance applies Algorithm 1 on the “flattened” and “paired” sequence of all of the workers’ paired-difference gradients, i.e.,

$$\mathbf{y}_{n(k-1)+i} = \mathbf{z}_{i,2k-1} - \mathbf{z}_{i,2k}, \quad \forall k \in \left[\frac{n}{2}\right], \quad i = 1 \dots m.$$

That is, we fit these ordered paired differences $\{\mathbf{y}_i\}_{i=1}^{mn/2}$ into the herding and balancing framework: If sign s is associated with $\mathbf{y}_{n(k-1)+i}$, then $\mathbf{z}_{i,2k-1}$ and $\mathbf{z}_{i,2k}$ receive s and $-s$, respectively.

3.3 The full-stack CD-GraB algorithm

Having solved the parallel herding problem with pair balancing, we now demonstrate how to bring everything together in an optimization context to *coordinate distributed gradient balancing* for distributed training. That is, we can now introduce our full-stack CD-GraB algorithm, which trains models in a distributed setting (Section 3.1) while efficiently ordering the examples by using PairBalance (Section 3.2, Algorithm 2) in an online manner. We describe CD-GraB at two levels of abstraction: a high-level illustration (Figure 1, steps 1–7) and a detailed pair of worker-server algorithm statements (Figure 2). Together, both show how CD-GraB enables distributing training across parallel workers: Since the workers only have access to a subset of the training data, in parallel they compute local, per-example stochastic gradients and send them to the server; the server simultaneously calls PairBalance online, which coordinates information from all the workers’ gradients, using adjacent example-specific gradients to determine the next epoch’s worker-specific permutations.

In more detail: In epoch t , (Figure 1, step 1) the two workers have permutations $\pi_{t,1}$ and $\pi_{t,2}$, respectively. Each worker computes per-example gradients \mathbf{g}_j^i (2; Algorithm 3:4), and sends them to the server (3; Algorithm 3:5). The server implements functions as a parameter server [20]: It computes the average of the workers’ per-example gradients (Algorithm 4:6), and sends it back to all workers (Algorithm 4:7) so that they can update their local models (Algorithm 3:6–7). Simultaneously, as the server receives gradients (Algorithm 4:5), it calls PairBalance (Algorithm 2) on adjacent vectors (4; Algorithm 4:4–13). PairBalance produces signs to supply to

Algorithm 3 CD-GraB Workers

require: m workers, $n := \frac{N}{m}$ ex. per worker
input: initial \mathbf{w}_1^1 , epochs T , learning rate α

```

1: receive: initial permutations  $\leftarrow \{\pi_{1,i}\}_{i=1}^m$ 
2: for epoch  $t := 1 \dots T$  do
  ▷ Run in parallel for workers  $i = 1 \dots m$ 
3:   for example  $j := 1 \dots n$  do
4:     compute:  $\mathbf{g}_j^i \leftarrow \nabla f^i(\mathbf{w}_t^j, \pi_{t,i}(j))$ 
5:     send:  $\mathbf{g}_j^i$   $\xrightarrow{j\text{-th stochastic grad. } \mathbf{g}_j^i}$ 
6:     receive:  $\bar{\mathbf{g}}_j$   $\xleftarrow{\text{avg. } j\text{-th stochastic grad. } \bar{\mathbf{g}}_j}$ 
7:     update:  $\mathbf{w}_t^{j+1} \leftarrow \mathbf{w}_t^j - \alpha \bar{\mathbf{g}}_j$ 
8:   end for
9:   receive: next permutation  $\leftarrow \pi_{t+1,i}$ 
10:  update:  $\mathbf{w}_{t+1}^1 := \mathbf{w}_t^{n+1}$ 
11: end for
12: return:  $\mathbf{w}_{T+1}^1 := \mathbf{w}_{T+1}^1$ 

```

Algorithm 4 CD-GraB Parameter Server

require: m workers, $n := \frac{N}{m}$ ex. per worker
input: epochs T

```

1: send: initial permutations  $\{\pi_{1,i}\}_{i=1}^m$ 
2: for epoch  $t := 1 \dots T$  do
3:   initialize: running sum  $\mathbf{h} = \mathbf{0}$ ; empty list  $\mathcal{S}$ 
4:   for example  $j := 1 \dots n$  do
5:     receive:  $\{\mathbf{g}_j^i\}_{i=1}^m$  from all workers  $i$ 
6:     compute: avg. gradient:  $\bar{\mathbf{g}}_j \leftarrow \frac{1}{m} \sum_{i=1}^m \mathbf{g}_j^i$ 
7:     send:  $\bar{\mathbf{g}}_j$  to all the workers
8:     for worker  $i := 1 \dots m$  do
9:       if  $j \bmod 2 = 0$ :
10:         $\mathbf{h}, s_{j-1}^i, s_j^i \leftarrow \text{PairBalance}(\mathbf{h}, \mathbf{g}_{j-1}^i, \mathbf{g}_j^i)$ 
11:         $\mathcal{S}.append(s_{j-1}^i); \mathcal{S}.append(s_j^i)$ 
12:      end for
13:   end for
  ▷ Call Alg. 1 for  $i = 1 \dots m$  on  $\pi_{t,i}$  and  $\mathcal{S}$ 
14:   compute: next permutations  $\{\pi_{t+1,i}\}_{i=1}^m$ 
15:   send:  $\{\pi_{t+1,i}\}_{i=1}^m$  to each worker  $i$ 
16: end for

```

Figure 2: CD-GraB worker and server (here, a parameter server [20]) algorithms.

the reordering algorithm (Algorithm 1), which, using the current worker permutations $\pi_{t,i}$, produces the new per-worker permutations for the next epoch (5; Algorithm 4:14). In Figure 1, these correspond to $\pi_{t+1,1}$ and $\pi_{t+1,2}$, which the server then sends back to the respective workers (6; Algorithm 4:15). Lastly, before the start of the next epoch, the workers reorder their examples according to the new permutations (7; Algorithm 3:9).

4 Convergence Analysis

We next demonstrate formally that our CD-GraB algorithm (Section 3.3) confers the efficiency benefits of centralized GraB (Section 2.1) to the distributed setting. In brief, our main theoretical results show that **CD-GraB enjoys a linear speedup in convergence rate** under two sets of conditions: smoothness (Theorem 1) and the Polyak-Łojasiewicz (P.L.) condition (Theorem 2). **Both results guarantee that CD-GraB is faster than distributed random reshuffling (D-RR)**; they rely on Alweiss et al. [2], which shows that RandomizedBalance (subroutine in Algorithm 2) guarantees a $\tilde{O}(1)$ bound to the signed herding objective (4). We summarize this dependency formally with

Statement 1. *For the RandomizedBalance subroutine in Algorithm 2 [2], there exists a constant $\tilde{A} = \tilde{O}(1)$ such that for any input vectors $\{\mathbf{z}_j\}_{j=1}^N$ with $\|\mathbf{z}_j\|_2 \leq 1$, RandomizedBalance outputs a sequence of signs $\{s_j\}_{j=1}^N \in \{-1, 1\}$ that fulfill*

$$\max_{k \in [N]} \left\| \sum_{j=1}^k s_j (\mathbf{z}_j - \bar{\mathbf{z}}) \right\|_{\infty} \leq \tilde{A}, \quad \text{with } \bar{\mathbf{z}} = \frac{1}{N} \sum_{i=1}^N \mathbf{z}_i.$$

Given the above, we prove a convergence guarantee for CD-GraB, beginning with a few assumptions:

Assumption 1 (Bounded Gradient Variance). $\forall i \in [m]$ there exists a constant $\sigma > 0$ such that

$$\forall j \in [N], \forall \mathbf{w} \in \mathbb{R}^d, \quad \text{it holds that} \quad \|\nabla f^i(\mathbf{w}, j) - \nabla f^i(\mathbf{w})\|_2^2 \leq \sigma^2.$$

Assumption 2 (Bounded Data Heterogeneity). There exists a constant $\varsigma > 0$ such that $\forall i \in [m]$,

$$\|\nabla f^i(\mathbf{w}) - \nabla f(\mathbf{w})\|_2^2 \leq \varsigma^2.$$

Assumption 3 (Smoothness). There exist constants $L_\infty > 0$ and $L_{2,\infty} > 0$ such that for any $\mathbf{w}, \mathbf{v} \in \mathbb{R}^d$ and any $i \in [m]$, it holds that

$$\|\nabla f^i(\mathbf{w}, j) - \nabla f^i(\mathbf{v}, j)\|_\infty \leq L_\infty \|\mathbf{w} - \mathbf{v}\|_\infty \quad \text{and} \quad \|\nabla f^i(\mathbf{w}, j) - \nabla f^i(\mathbf{v}, j)\|_2 \leq L_{2,\infty} \|\mathbf{w} - \mathbf{v}\|_\infty$$

Remarks on assumptions. Assumption 1 and 2 are standard in the distributed optimization community. Per Assumption 1, the deviation of the gradient of each local loss function $\nabla f^i(\mathbf{w}, j)$ from the average local loss gradient $\nabla f^i(\mathbf{w})$ (or, worker gradient) is uniformly bounded. Assumption 2 similarly bounds the deviation of the workers' gradients from the global gradient $\nabla f(\mathbf{w})$. Our assumptions **only** work with uniform boundedness, but not in-expectation boundedness, a requirement that comes from herding. In return, we get deterministic convergence rate upper-bounds. For Assumption 3, we follow the original GraB paper [24] and assume a cross norm $L_{2,\infty}$.⁷

The convergence bound of CD-GraB is as follows:

Theorem 1. If Assumptions 1, 2 and 3 hold, and we set α to be

$$\alpha = \min \left\{ \frac{1}{16L_{2,\infty}(2n + \tilde{A}/m)}, \left(\frac{4F_1m^2}{42L_{2,\infty}^2(\varsigma + \sigma)^2\tilde{A}^2nT + 18L_{2,\infty}^2m^2n^3\sigma^2} \right)^{1/3} \right\}, \quad \text{then}$$

$$\frac{1}{T} \sum_{t=1}^T \|\nabla f(\mathbf{w}_t)\|_2^2 \leq \frac{9(F_1L_{2,\infty}(\varsigma + \sigma)\tilde{A})^{2/3}}{(mnT)^{2/3}} + \frac{(72F_1L_{2,\infty}\sigma)^{2/3} + 64F_1L_{2,\infty}(2 + \tilde{A}/(mn))}{T}$$

$$= \tilde{O} \left(\frac{1}{(mnT)^{2/3}} + \frac{1}{T} \right), \quad \text{where } F_1 = f(\mathbf{w}_1) - \inf_{\mathbf{w} \in \mathbb{R}^d} f(\mathbf{w}).$$

We can also prove an accelerated rate for CD-GraB if we additionally assume the P.L. condition:

Assumption 4 (P.L. Condition). We say the loss function f fulfills the P.L. condition if there exists $\mu > 0$ such that for any $\mathbf{w} \in \mathbb{R}^d$,

$$\frac{1}{2} \|\nabla f(\mathbf{w})\|_2^2 \geq \mu(f(\mathbf{w}) - \inf_{\mathbf{v} \in \mathbb{R}^d} f(\mathbf{v})).$$

Theorem 2. If Assumptions 1-4 hold, and we set learning rate α and constants \tilde{W} and C_3 to

$$C_3 = \frac{(F_1 + \sigma^2/L_{2,\infty})\mu^2}{224L_{2,\infty}^2(\varsigma + \sigma)^2\tilde{A}^2} \quad \tilde{W} = W_0(T^2m^2n^2C_3) \quad \alpha = \frac{2\tilde{W}}{Tn\mu},$$

where W_0 is the Lambert-W function; then, if the number of epochs T satisfies

$$T \geq 10 + \frac{1}{\mu} 32L_{2,\infty}(2 + \tilde{A}/(mn))W_0((mnT)^2C_3) = \tilde{O}(1), \quad \text{it holds that}$$

$$F_{T+1} \leq \frac{1}{(mnT)^2} \left(\frac{(F_1 + L_{2,\infty}^2\sigma^2)\tilde{W}}{C_3} + \frac{112L_{2,\infty}^2(\varsigma + \sigma)^2\tilde{A}^2\tilde{W}^2}{\mu^3} \right) = \tilde{O} \left(\frac{1}{(mnT)^2} \right),$$

where $F_{T+1} = f(\mathbf{w}_{T+1}) - \inf_{\mathbf{w} \in \mathbb{R}^d} f(\mathbf{w})$.

These theorems prove that CD-GraB exhibits a linear speedup over GraB [24]'s $\tilde{O}((nT)^{-2/3})$ rate,⁸ in the number of workers m , under both smoothness and the P.L. condition (Appendix). Further, CD-GraB convergence rate of $\tilde{O}((mnT)^{-2})$ is faster than many previous rates,⁹ notably, prior work on D-RR: Yun et al. [48]'s high probability bound of $\tilde{O}((mn)^{-1}T^{-2})$ and the bound of $\tilde{O}((mT)^{-2}n^{-1})$ that uses a synchronized shuffling trick.

⁷This assumption can be easily adapted to L_2 -smoothness by setting $L_{2,\infty}$ to be $\sqrt{d}L_2$.

⁸For centralized GraB, the total number of examples $N = n$ and $m = 1$.

⁹These exclusively focus on the P.L. case, so we compare CD-GraB to them under the same condition.

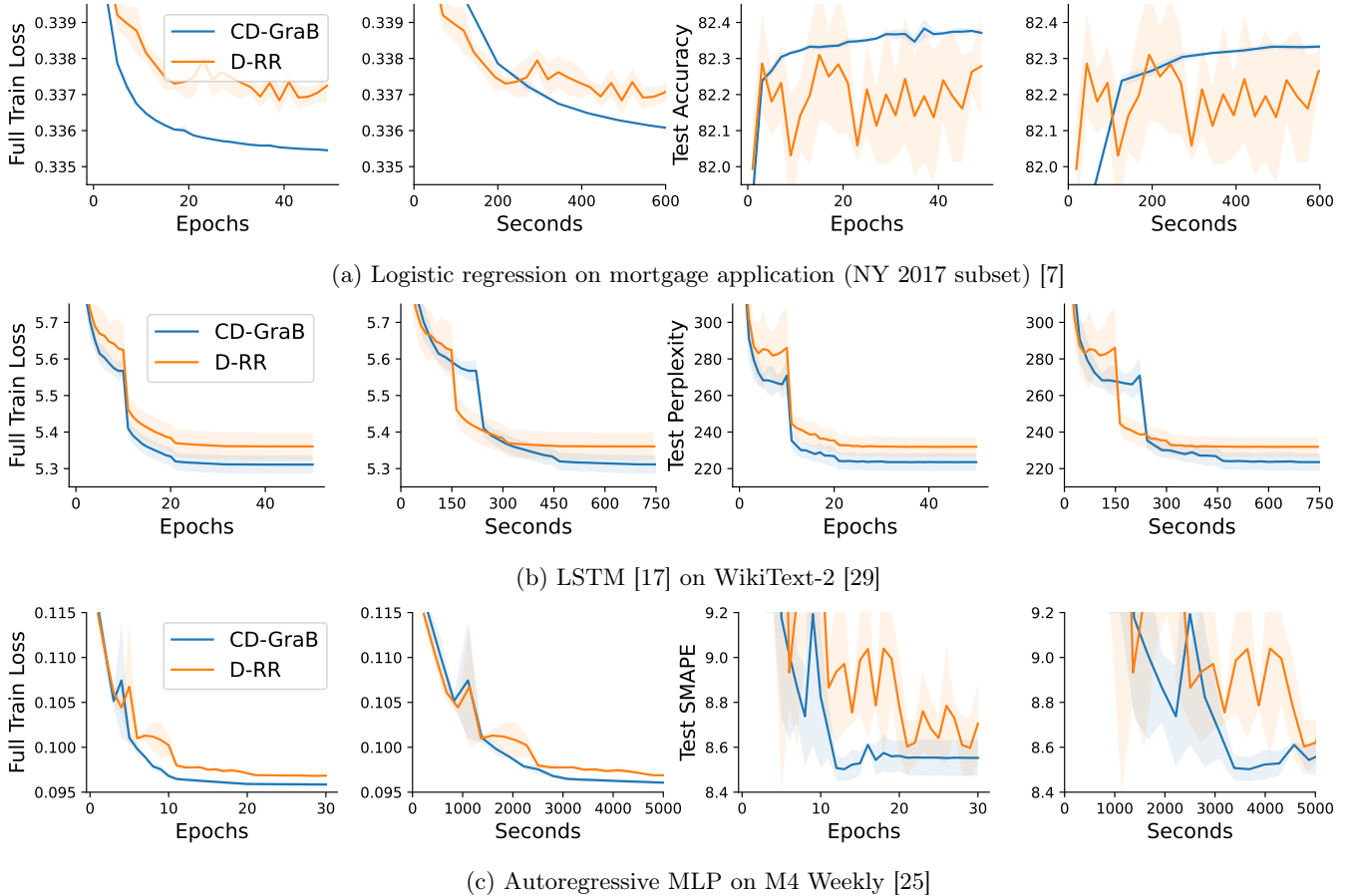


Figure 3: Convergence of CD-GraB in comparison to D-RR. For each experiment, we show train loss over epochs and time (**left** of each subfigure) and test performance over epochs and time (**right** of each subfigure). We run 3 random seeds, and plot the mean \pm STD.

5 CD-GraB in Practice: Distributed and Simulation Experiments

We next verify CD-GraB’s accelerated convergence on a variety of large-scale empirical tasks. We also run an ablation study to isolate the effects of different improvements in CD-GraB. We do this because online PairBalance exhibits performance benefits are separate from parallelism — namely, removing the need for gradient centering with a stale mean and allowing for higher learning rates (Section 3.2).¹⁰

Evaluating CD-GraB’s convergence speedup. We use the following three tasks for evaluating distributed training efficiency: logistic regression on a large-scale mortgage application (New York 2017 subset, 244,107 examples with 18 features) [7] (Figure 3a), Long Short-Term Memory (LSTM) [17] on the WikiText-2 dataset [29] (Figure 3b), and autoregressive Multi-Layer Perceptron (MLP) on the M4 Weekly dataset [25] (Figure 3c). We measure the loss incurred on the entire training set (Full Train Loss) and task-appropriate test metrics during evaluation, with respect to both the number of epochs and wall-clock time. Regarding test metrics, we measure test accuracy for the mortgage application, perplexity for WikiText-2, and SMAPE for M4. Additional details regarding the datasets, models, and test metrics can be found in the Appendix.

For all three tasks, we use a single 128 GiB memory machine with 4 NVIDIA GeForce RTX 2080 Ti GPUs. For the mortgage application and WikiText-2 (Figures 3a and 3b), we launch $m = 4$ workers (processes), where each worker runs on one GPU. For the M4 task, we launch $m = 32$ workers, where each of the 4 GPUs hosts 8 process workers. We use NCCL as the distributed communication backend [33] for the mortgage application and

¹⁰GraB can also implement online PairBalance, in place of Balance [22], for empirical improvements.

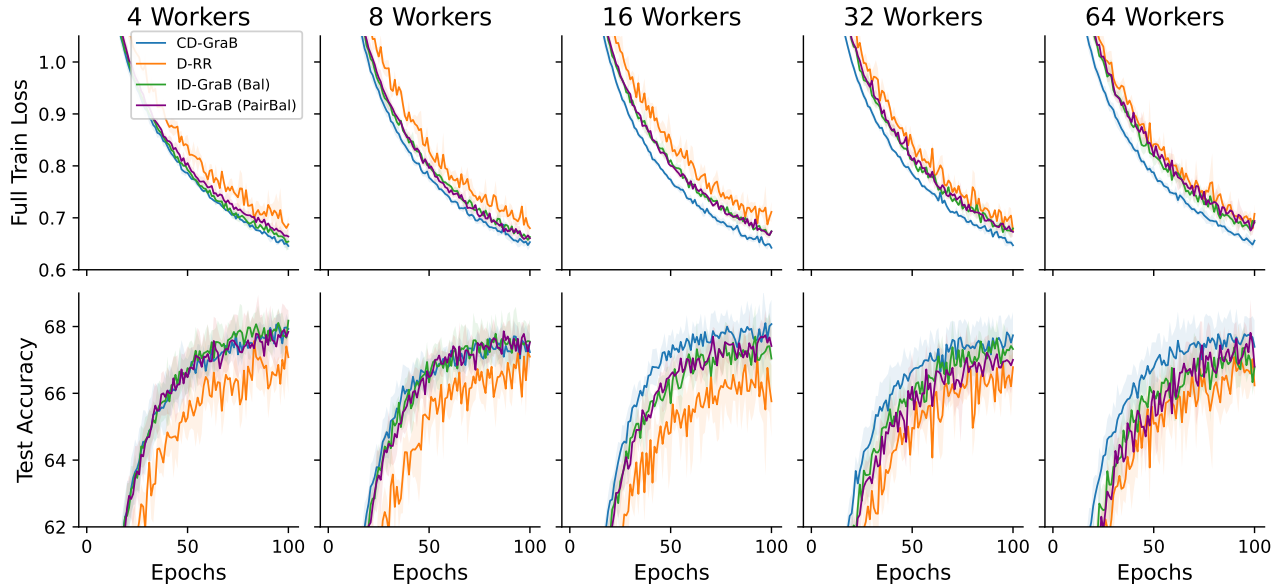


Figure 4: Convergence for CD-GraB, D-RR, ID-GraB (Bal), and ID-GraB (PairBal) training LeNet on CIFAR-10, with $m \in \{4, 8, 16, 32, 64\}$ workers. For each, the aggregated minibatch size per update is 64.

WikiText-2 tasks, and GLOO [1] as the distributed communication backend for M4 task.¹¹As shown in Figure 3, we compare CD-GraB’s convergence to the standard distributed training example ordering method: random reshuffling (D-RR). From all subfigures in Figure 3, we observe that CD-GraB outperforms the D-RR baseline significantly and consistently: CD-GraB exhibits better training loss and test metrics, measured against both the number of epochs and wall-clock time.

Ablation simulation study: The importance of coordination at large scale. CD-GraB has several design benefits over the original centralized GraB algorithm [24]: Coordinating parallel workers’ specific permutations using *PairBalance* on the server (Algorithm 2) and removing the dependency on a stale mean (Section 2.1), which enables the ability to using larger learning rates reliably (Section 3.2). Clearly, not all of these benefits come directly from distributing training. For example, being able to use larger learning rates, is a side effect of our solution to develop CD-GraB, not our main contribution. Therefore, we run a simulation ablation study to disentangle the relative importance of each of CD-GraB’s efficiency benefits over GraB. To do so, we compare the convergence of CD-GraB to two additional baselines in the distributed setting, beyond D-RR: (1) **ID-GraB (Bal)**, where each independent worker runs GraB locally using *RandomizedBalance* (subroutine in Algorithm 2) to perform gradient vector balancing; (2) **ID-GraB (PairBal)**, where each independent worker runs GraB locally using *PairBalance*.

We summarize the results in Figure 4, for which we show convergence curves for $m \in \{4, 8, 16, 32, 64\}$ workers training LeNet on CIFAR-10. We choose this task and architecture to cohere with the experiments done in the original GraB paper. We make two main observations. First, when scaling up training with more workers, CD-GraB converges increasingly faster than the no-coordination-ordering methods **ID-GraB (Bal)** and **ID-GraB (PairBal)**. This result aligns with our theory and intuition that, when the number of workers m increases, the parallel herding bound (8) will increase linearly if there is no coordination. Second, as we scale up to larger m , the convergence curves of **ID-GraB (Bal)** and **ID-GraB (PairBal)** gradually approach the curve for D-RR. This indicates that, at larger scales, herding-based example ordering will be no better than randomly permuting the dataset. Both observations give strong evidence that coordination in CD-GraB, i.e., running online *PairBalance* on the server side to coordinate per-worker permutations is critical for accelerating training.

¹¹We discard $N \bmod B$ (B is aggregated minibatch size) examples at random to ensure n examples per worker.

6 Conclusion and Future Work: Toward an Order Server Architecture

We elevate the benefits of provably faster, permutation-based example ordering to the contemporary ML distributed training setting. We focus on reformulating the online **G**radient **B**alancing algorithm (GraB) [24] because, even though it is the provably optimal permutation-based example ordering method [6], it is limited by design to *centralized* settings (Section 3.1). To overcome these limitations, we redesign GraB’s herding and balancing framework to account for parallel workers: A *parallel herding* objective, which we solve with an online PairBalance subroutine, based on key insights in kernel thinning [3, 10, 11]. PairBalance operates on ordered *pairs* of vectors to do balancing, which enables our full-stack, low-overhead, *C*oordinated and *D*istributed online CD-GraB algorithm. We give a full specification of our online CD-GraB algorithm (Section 3.3), provide convergence rate guarantees regarding its speedups on both smooth non-convex and P.L. objectives (Section 4), and verify these speedups in practice on single-node distributed tasks and a simulated ablation study (Section 5).

Both our theory and experiments demonstrate that CD-GraB really shines when there are multiple training epochs (Appendix). We therefore do not include experiments involving fine-tuning pre-trained models like GPT, as fine-tuning can be achieved in just a couple of epochs. Pre-training from scratch would demonstrate the tremendous power of CD-GraB to scale to very large models; however, we did not have the training budget to perform such experiments for the present work.

Further, to truly exercise the benefits of CD-GraB in such large-scale settings, future work should investigate moving beyond the single-node setup that we present. Notably, to train larger models, our results suggest a novel distributed training architecture. The ordering operation performed by the server (Algorithm 4) is *not* very latency sensitive; the server has the duration of the entire epoch t to compute the new permutations for the next, $t + 1$ epoch. Given this relaxed latency requirement, and the success of our algorithmic results, it would be an exciting direction for future ML systems research to invest in building an *Order Server* architecture. Such an architecture, which could be composed with traditional parameter servers, would afford the scalability benefits of CD-GraB to a host of massive-scale ML applications.

Acknowledgments

A. Feder Cooper is supported by Christopher De Sa’s NSF CAREER grant, and in part by the Artificial Intelligence Policy and Practice initiative at Cornell University and the John D. and Catherine T. MacArthur Foundation. Yucheng Lu is supported by Meta Ph.D. Fellowship. We also acknowledge a gift from SambaNova Systems.

References

- [1] Collective communications library with various primitives for multi-machine training, 2023. URL <https://github.com/facebookincubator/gloo>.
- [2] Ryan Alweiss, Yang P Liu, and Mehtaab Sawhney. Discrepancy minimization via a self-balancing walk. In *Proceedings of the 53rd Annual ACM SIGACT Symposium on Theory of Computing*, pages 14–20, 2021.
- [3] Alessandro Barp, Carl-Johann Simon-Gabriel, Mark Girolami, and Lester Mackey. Targeted separation and convergence with kernel discrepancies. *arXiv preprint arXiv:2209.12835*, 2022.
- [4] Dimitri P. Bertsekas. Incremental Gradient, Subgradient, and Proximal Methods for Convex Optimization: A Survey. In *Optimization for Machine Learning*. The MIT Press, 2011.
- [5] Léon Bottou. Stochastic gradient descent tricks. In *Neural networks: Tricks of the trade*, pages 421–436. Springer, 2012.
- [6] Jaeyoung Cha, Jaewook Lee, and Chulhee Yun. Tighter Lower Bounds for Shuffling SGD: Random Permutations and Beyond, 2023.
- [7] A. Feder Cooper, Solon Barocas, Christopher De Sa, and Siddhartha Sen. Variance, Self-Consistency, and Arbitrariness in Fair Classification. *arXiv preprint arXiv:2301.11562*, 2023.

- [8] Christopher De Sa. Random Reshuffling is Not Always Better. In *Advances in Neural Information Processing Systems*, 2020.
- [9] Jacob Devlin, Ming-Wei Chang, Kenton Lee, and Kristina Toutanova. BERT: Pre-training of Deep Bidirectional Transformers for Language Understanding. In *Proceedings of the 2019 Conference of the North American Chapter of the Association for Computational Linguistics: Human Language Technologies, Volume 1 (Long and Short Papers)*, pages 4171–4186, 2019.
- [10] Raaz Dwivedi and Lester Mackey. Kernel thinning. *arXiv preprint arXiv:2105.05842*, 2021.
- [11] Raaz Dwivedi and Lester Mackey. Generalized Kernel Thinning. In *Tenth International Conference on Learning Representations*, 2022.
- [12] Alex Graves, Marc G Bellemare, Jacob Menick, Remi Munos, and Koray Kavukcuoglu. Automated curriculum learning for neural networks. In *international conference on machine learning*, pages 1311–1320. PMLR, 2017.
- [13] Mert Gürbüzbalaban, Asuman E. Ozdaglar, and Pablo A. Parrilo. Convergence Rate of Incremental Gradient and Incremental Newton Methods. *SIAM Journal on Optimization*, 29(4):2542–2565, 2019.
- [14] Mert Gürbüzbalaban, Asu Ozdaglar, and Pablo A Parrilo. Why random reshuffling beats stochastic gradient descent. *Mathematical Programming*, 186(1):49–84, 2021.
- [15] Jeff Z. HaoChen and Suvrit Sra. Random Shuffling Beats SGD after Finite Epochs. In *Proceedings of the International Conference on Machine Learning*, volume 97, pages 2624–2633, 2019.
- [16] Nick Harvey and Samira Samadi. Near-Optimal Herding. In *Proceedings of The 27th Conference on Learning Theory*, volume 35, pages 1165–1182, 2014.
- [17] Sepp Hochreiter and Jürgen Schmidhuber. Long short-term memory. *Neural computation*, 9(8):1735–1780, 1997.
- [18] Kun Huang, Xiao Li, Andre Milzarek, Shi Pu, and Junwen Qiu. Distributed Random Reshuffling over Networks. *arXiv preprint arXiv:2112.15287*, 2021.
- [19] Hakan Inan, Khashayar Khosravi, and Richard Socher. Tying word vectors and word classifiers: A loss framework for language modeling. *arXiv preprint arXiv:1611.01462*, 2016.
- [20] Mu Li, David G. Andersen, Jun Woo Park, Alexander J. Smola, Amr Ahmed, Vanja Josifovski, James Long, Eugene J. Shekita, and Bor-Yiing Su. Scaling Distributed Machine Learning with the Parameter Server. In *Proceedings of the 11th USENIX Conference on Operating Systems Design and Implementation*, OSDI’14, page 583–598, USA, 2014. USENIX Association. ISBN 9781931971164.
- [21] Ilya Loshchilov and Frank Hutter. Decoupled weight decay regularization. *arXiv preprint arXiv:1711.05101*, 2017.
- [22] Yucheng Lu, Si Yi Meng, and Christopher De Sa. A General Analysis of Example-Selection for Stochastic Gradient Descent. In *International Conference on Learning Representations*, 2021.
- [23] Yucheng Lu, Youngsuk Park, Lifan Chen, Yuyang Wang, Christopher De Sa, and Dean Foster. Variance Reduced Training with Stratified Sampling for Forecasting Models. In *Proceedings of the International Conference on Machine Learning*, pages 7145–7155. PMLR, 2021.
- [24] Yucheng Lu, Wentao Guo, and Christopher De Sa. GraB: Finding Provably Better Data Permutations than Random Reshuffling. In Alice H. Oh, Alekh Agarwal, Danielle Belgrave, and Kyunghyun Cho, editors, *Advances in Neural Information Processing Systems*, 2022. URL <https://openreview.net/forum?id=nDemfqKHTpK>.
- [25] Spyros Makridakis, Evangelos Spiliotis, and Vassilios Assimakopoulos. The m4 competition: 100,000 time series and 61 forecasting methods. *International Journal of Forecasting*, 36(1):54–74, 2020. ISSN 0169-2070. doi: <https://doi.org/10.1016/j.ijforecast.2019.04.014>. URL <https://www.sciencedirect.com/science/article/pii/S0169207019301128>. M4 Competition.

- [26] Grigory Malinovsky, Konstantin Mishchenko, and Peter Richtárik. Server-Side Stepsizes and Sampling Without Replacement Provably Help in Federated Optimization. *arXiv preprint arXiv:2201.11066*, 2022.
- [27] Tabet Matiisen, Avital Oliver, Taco Cohen, and John Schulman. Teacher–student curriculum learning. *IEEE transactions on neural networks and learning systems*, 31(9):3732–3740, 2019.
- [28] Brendan McMahan, Eider Moore, Daniel Ramage, Seth Hampson, and Blaise Aguera y Arcas. Communication-efficient learning of deep networks from decentralized data. In *Artificial intelligence and statistics*, pages 1273–1282. PMLR, 2017.
- [29] Stephen Merity, Nitish Shirish Keskar, and Richard Socher. Regularizing and optimizing lstm language models. In *International Conference on Learning Representations*, 2018.
- [30] Konstantin Mishchenko, Ahmed Khaled, and Peter Richtárik. Random Reshuffling: Simple Analysis with Vast Improvements. In *Advances in Neural Information Processing Systems*, 2020.
- [31] Amirkeivan Mohtashami, Sebastian Stich, and Martin Jaggi. Characterizing & Finding Good Data Orderings for Fast Convergence of Sequential Gradient Methods. *arXiv preprint arXiv:2202.01838*, 2022.
- [32] Deanna Needell, Rachel Ward, and Nathan Srebro. Stochastic Gradient Descent, Weighted Sampling, and the Randomized Kaczmarz algorithm. In *Advances in Neural Information Processing Systems*, pages 1017–1025, 2014.
- [33] NVIDIA. NVIDIA Collective Communication Library, 2023. URL <https://developer.nvidia.com/ncc1>.
- [34] PyTorch Contributors. DataLoader API, 2023. URL <https://pytorch.org/docs/stable/data.html>.
- [35] Alec Radford, Jeff Wu, Rewon Child, David Luan, Dario Amodei, and Ilya Sutskever. Language models are unsupervised multitask learners. 2019.
- [36] Shashank Rajput, Kangwook Lee, and Dimitris Papailiopoulos. Permutation-Based SGD: Is Random Optimal? In *International Conference on Learning Representations*, 2022.
- [37] Benjamin Recht and Christopher Ré. Toward a Noncommutative Arithmetic-geometric Mean Inequality: Conjectures, Case-studies, and Consequences. In *Conference on Learning Theory*, volume 23, pages 11.1–11.24, 2012.
- [38] Abdurakhmon Sadiev, Grigory Malinovsky, Eduard Gorbunov, Igor Sokolov, Ahmed Khaled, Konstantin Burlachenko, and Peter Richtárik. Federated Optimization Algorithms with Random Reshuffling and Gradient Compression. *arXiv preprint arXiv:2206.07021*, 2022.
- [39] Mark Schmidt, Nicolas Le Roux, and Francis R. Bach. Minimizing finite sums with the stochastic average gradient. *Mathematical Programming*, 162(1-2):83–112, 2017.
- [40] Samuel L Smith, Pieter-Jan Kindermans, Chris Ying, and Quoc V Le. Don’t Decay the Learning Rate, Increase the Batch Size. In *International Conference on Learning Representations*, 2018.
- [41] Petru Soviany, Radu Tudor Ionescu, Paolo Rota, and Nicu Sebe. Curriculum learning: A survey. *International Journal of Computer Vision*, pages 1–40, 2022.
- [42] Evangelos Spiliotis, Andreas Kouloumos, Vassilios Assimakopoulos, and Spyros Makridakis. Are forecasting competitions data representative of the reality? *International Journal of Forecasting*, 36(1):37–53, 2020.
- [43] Merity Stephen, Xiong Caiming, Bradbury James, and Richard Socher. Pointer sentinel mixture models. *Proceedings of ICLR*, 2017.
- [44] Alex Wang, Amanpreet Singh, Julian Michael, Felix Hill, Omer Levy, and Samuel Bowman. GLUE: A multi-task benchmark and analysis platform for natural language understanding. In *Proceedings of the 2018 EMNLP Workshop BlackboxNLP: Analyzing and Interpreting Neural Networks for NLP*, pages 353–355, Brussels, Belgium, November 2018. Association for Computational Linguistics. doi: 10.18653/v1/W18-5446. URL <https://aclanthology.org/W18-5446>.

- [45] Max Welling. Herding dynamical weights to learn. In *Proceedings of the 26th Annual International Conference on Machine Learning*, pages 1121–1128, 2009.
- [46] Bicheng Ying, Kun Yuan, Stefan Vlaski, and Ali H. Sayed. On the performance of random reshuffling in stochastic learning. In *2017 Information Theory and Applications Workshop (ITA)*, pages 1–5. IEEE, 2017.
- [47] Binhang Yuan, Yongjun He, Jared Davis, Tianyi Zhang, Tri Dao, Beidi Chen, Percy S Liang, Christopher Re, and Ce Zhang. Decentralized training of foundation models in heterogeneous environments. *Advances in Neural Information Processing Systems*, 35:25464–25477, 2022.
- [48] Chulhee Yun, Shashank Rajput, and Suvrit Sra. Minibatch vs Local SGD with Shuffling: Tight Convergence Bounds and Beyond. In *International Conference on Learning Representations*, 2021.
- [49] Chulhee Yun, Suvrit Sra, and Ali Jadbabaie. Open Problem: Can Single-Shuffle SGD be Better than Reshuffling SGD and GD? In *Conference on Learning Theory*, 2021.

A Glossary

Term/Symbol	Explanation
GraB	Centralized online Gradient Balancing algorithm. We use this term to refer to the centralized algorithm developed in the original GraB paper (Lu et al. [24]).
CD-GraB	Coordinated and distributed online Gradient Balancing algorithm. We use this term to refer to the algorithm that constitutes our main contribution.
ID-GraB	Independent and distributed online gradient balancing. We implement this for our ablation study, to compare with coordinated and distributed GraB. There are two variants: One which uses the original GraB paper’s online Balance algorithm (ID-GraB (Bal)), and one which implements our online PairBalance algorithm (ID-GraB (Bal)).
RR	Random reshuffling algorithm. We use this to refer to its centralized variant.
D-RR	Distributed random reshuffling algorithm.
SO	Shuffle Once algorithm.
\mathbf{x}	Data example vector; we do not use this in the math in the main paper, but do refer to examples in our schematic description for PairBalance ordering in Figure 1.
\mathbf{z}	Example vector (for illustration under the herding context).
$\bar{\mathbf{z}}$	The average example vector (for illustration under the herding context).
z_j	The j -th component of the example vector (for illustration under the herding context).
$z_{i,j}$	The j -th component of the example vector on worker i (for illustration under the parallel herding context).
\mathbf{w}	Parameters / model weights vector.
f	Loss function.
π	A permutation; we study permutation-based example orderings.
T	Number of epochs.
t	Index for iterating over T epochs.
m	Number of workers (in this paper, workers are always different GPUs on the same node).
i	Index for iterating over m workers .
n	Number of training data examples per worker; equivalent to $\frac{N}{m}$.
N	Number of total training data examples. $N = n$ in the centralized setting.
j	Index for iterating over examples (the N in the centralized setting, the n in the per-worker, distributed setting).
\mathbf{g}	Gradient, taken with respect to the model weights \mathbf{w} and data examples \mathbf{x} .
\mathbf{g}_j^i	Gradient associated with the j -th data example \mathbf{x} on worker i .
s	A sign, either +1 or −1; related to the signed herding problem.
s_j^i	A sign, either +1 or −1, computed according to the j -th example gradient \mathbf{g}_j^i for worker i ; to be associated with the example \mathbf{x}_j when determining a permutation ordering using Algorithm 1.

B Additional Details on the CD-GraB Algorithm

In this Appendix, we provide more details on related work and our contributions. To start, we provide unified description of our online CD-GraB algorithm with prior work on herding, vector balancing, and kernel thinning (Appendix B.1), some more details on Alweiss et al. [2] (that we elide in the main paper due to space constraints)

B.1 Distinguishing our contributions

We summarize our contributions in relation to prior work in a concise format. This kind of presentation would not be easily understandable without the appropriate background and context that we provide in the paper. This is why present it here, in the Appendix, so that (ideally) this is seen by the reader after finishing the main paper.

We emphasize that it is prior work that:

- Formulates the herding objective and solving it with vector balancing [16, 45] (Algorithm 1)
- Leverages ideas from herding and vector balancing (above) in an *online* fashion and in an optimization setting to do permutation-based example ordering [24]
- Observes and proves that it is possible to solve the herding objective in $\tilde{O}(1)$ by only examining differences on pairs of examples (the overarching idea of PairBalance [10], which relies on the RandomizedBalance subroutine [2]; see Algorithm 2)

Our contributions are to bring together all of this prior work in a novel way. We

- Translate herding to the parallel setting via defining a parallel herding objective (8)
- Leverage prior work on herding in an optimization setting [24] so that we can do parallel herding in an optimization setting (Section 3)
- Execute *online* pair balancing on a server (Algorithm 2 on a running sum, Figure 1), i.e., do pair balancing in a streaming and asynchronous (rather than blocking) fashion from gradient vectors produced on distributed workers (Algorithm 2), on the flattened sequenced of paired-difference gradients (Section 3.2)

B.2 More details on RandomizedBalance from Alweiss et al. [2]

In the subroutine for RandomizedBalance in Algorithm 2, we elide details about how the probability p is computed exactly as in Alweiss et al. [2]. We provide the more complete specification in Algorithm 5 written in terms of a single input vector (which, for us, is the vector containing the difference between adjacent gradients). Note that the difference here is in the use of a required parameter, constant upper bound w , which is used to compute the probability p . For clarity of presentation in the subroutine in Algorithm 2, we have set $w = 1$.

Algorithm 5 Probabilistic Balancing with Logarithm Bound [Alweiss et al. [2]]

```
require: parameter  $w$ , used to compute probability  
input: current running sum  $\mathbf{r}$  vector, vector  $\mathbf{z}_{\text{diff}}$   
1: if  $|\langle \mathbf{r}, \mathbf{z}_{\text{diff}} \rangle| > w$  or  $\|\mathbf{r}\|_{\infty} > w$  then  
2:   Fail  
3: end if  
4: compute:  $p \leftarrow \frac{1}{2} - \frac{\langle \mathbf{r}, \mathbf{z}_{\text{diff}} \rangle}{2w}$   
5: compute:  $s \leftarrow +1$  with probability  $p$ ;  
    $s \leftarrow -1$  with probability  $1 - p$   
6: update:  $\mathbf{r} \leftarrow \mathbf{r} + s\mathbf{z}_{\text{diff}}$   
7: return:  $s, \mathbf{r}$ 
```

In practice, we actually do not use RandomizedBalance in our online PairBalance. We use the deterministic greedy ordering algorithm from the original Lu et al. [24, Algorithm 5] paper:

Algorithm 6 Balancing without normalization [Lu et al. [24]]

input: current running sum \mathbf{r} vector, vector \mathbf{z}_{diff}
1: **if** $\|\mathbf{r} + \mathbf{z}_{\text{diff}}\| < \|\mathbf{r} - \mathbf{z}_{\text{diff}}\|$ **then** $s \leftarrow +1$ **else** $s \leftarrow -1$
2: **update:** $\mathbf{r} \leftarrow \mathbf{r} + s\mathbf{z}_{\text{diff}}$
3: **return:** s, \mathbf{r}

B.3 Implementing CD-GraB with a parameter server

For our implementation of CD-GraB, we use a parameter server architecture [20]. For our purposes, this just entails computing the average gradient (used to update the model on all workers) on the server side. That is, the server (other than determining the ordering for the next epoch) also has the function of aggregating gradient information (in this case, a simple mean) to send back to the workers. We have the server compute the average j -th gradient for illustrative purposes. We could, instead, implement the computation the average gradient as an all-reduce operation, in which each worker broadcasts their gradients to all other workers, so that they can each locally compute the average gradient to update their local models. We implement CD-GraB using a parameter server pattern to show that this is a plausible architecture to use with our coordinated and distributed example ordering algorithm. We could also implement a full parameter server system, for which the server also coordinates global model updates.

If we kept everything in our implementation the same and switched to all-reduce, then we would no longer be following a parameter server paradigm. In this case, the server would just function to determine example orders. It is this kind of paradigm that suggests the abstraction of an *order server*, which we mention briefly in Section 6: A server whose sole responsibility is coordinating worker information to determine example ordering.

In future work, we intend to explore a host of architectural possibilities — of building a full system that incorporates both traditional parameter server aspects with our new abstraction of an order server. For example, we could have parameter servers and order servers work in tandem in a distributed system to perform model training. To move beyond the single-node implementation we present in this paper, we intend to investigate the benefits and trade-offs associated with such design decisions in an actual implemented system.

B.4 Centralized online PairBalance

In Section 3.3, we provide a schematic diagram of how online PairBalance works for a distributed implementation using a parameter server (Figure 1). We also claim in Section 3 that online PairBalance can be applied to the original centralized GraB algorithm for improved empirical performance. We provide a schematic here, in Figure 5 (analogous to Figure 1), for how online PairBalance for centralized GraB.

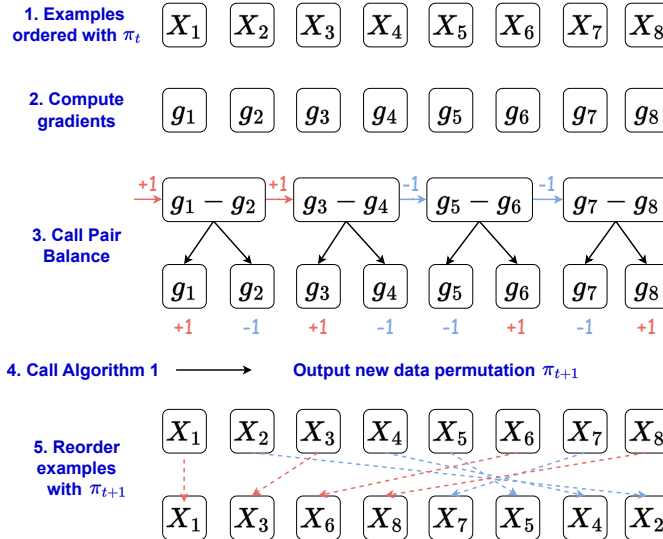


Figure 5: Schematic representation of online PairBalance for centralized GraB.

C Proof Results

We present supporting results, which we use to prove the main results presented in Section 4.

C.1 Analyzing the parallel herding bound

In the main paper, we cover how CD-GraB runs on both the worker- and server-side. In this section, we dive deep into the example ordering part of CD-GraB, and demonstrate in theory how server-side **PairBalance** reduces the parallel herding bound (8), as formulated in Section 3. We conclude this section by presenting Lemma 1, which shows server-side **PairBalance** is able to reduce the parallel herding bound iteratively.

We formalize our illustration over a group of vectors (since vector balancing, including **PairBalance**, does not inherently involve optimization context until we use it in our online setting).

Given a set of vectors $\mathbf{z}_{i,j} \in \mathbb{R}^d$ for $i \in [m]$ and $j \in [n]$ evenly located on m workers (i.e., $n = \frac{N}{m}$), where $\mathbf{z}_{i,j}$ denotes the j -th vector located on the i -th worker. Now denote π_i as the original permutation of the vectors on worker i . Consider running Algorithm 7 on the server side over these vectors:

Algorithm 7 Server-side **PairBalance** over a set of vectors (one step)

```

require:  $m$  workers,  $n := \frac{N}{m}$  vectors per worker
input: initial permutations from all the workers  $\{\pi_i\}_{i=1}^m$ 
1: initialize: new permutations from all the workers  $\{\pi'_i\}_{i=1}^m$ 
2: initialize: running partial sum  $\mathbf{h} = 0$ 
3: initialize: new indices front (left) pointer  $\{l_i = 1\}_{i=1}^m$ 
4: initialize: new indices back (right) pointer  $\{r_i = 1\}_{i=1}^m$ 
5: for example  $j := 1 \dots n$  do
6:   for worker  $i := 1 \dots m$  do
7:     if  $j \bmod 2 = 0$  then
8:        $\mathbf{h}, s_{j-1}^i, s_j^i \leftarrow \text{PairBalance}(\mathbf{h}, \mathbf{z}_{j-1}^i, \mathbf{z}_j^i)$ 
9:       if  $s_{j-1}^i = +1$  then
10:         $\pi'_i(l_i) = j - 1; \quad l_i = l_i + 1$ 
11:         $\pi'_i(r_i) = j; \quad r_i = r_i - 1$ 
12:       else
13:         $\pi'_i(l_i) = j; \quad l_i = l_i + 1$ 
14:         $\pi'_i(r_i) = j - 1; \quad r_i = r_i - 1$ 
15:       end if
16:     end if
17:   end for
18: end for
19: output: new permutations for all  $m$  workers  $\{\pi'_i\}_{i=1}^m$ 

```

Figure 6: One-step **PairBalance** algorithm on the server side to solve the parallel herding problem (8). This algorithm can be seen as a prototype for Algorithm 4 and Algorithm 3, without the optimization context.

It follows, in the following Lemma 1, that we can get the parallel herding bound with the output permutations $\{\pi'_i\}_{i=1}^m$:

Lemma 1. *Given a set of vectors $\mathbf{z}_{i,j} \in \mathbb{R}^d$ for $i \in [m]$ and $j \in [n]$ that satisfies:*

$$\left\| \sum_{i=1}^m \sum_{j=1}^n \mathbf{z}_{i,j} \right\|_{\infty} \leq c_1 \quad \text{and} \quad \left\| \mathbf{z}_{i',j'} - \frac{1}{N} \sum_{i=1}^m \sum_{j=1}^n \mathbf{z}_{i,j} \right\|_{\infty} \leq c_2 \quad \forall i' \in [m], \quad j' \in [n]$$

for some constants $c_1 > 0$ and $c_2 > 0$. Suppose we run Algorithm 7 over these vectors, then it holds that:

$$\max_{l \in [n]} \left\| \sum_{i=1}^m \sum_{j=1}^l \mathbf{z}_{i, \pi'_i(j)} \right\|_{\infty} \leq \frac{1}{2} \max_{l \in [n]} \left\| \sum_{i=1}^m \sum_{j=1}^l \mathbf{z}_{i, \pi_i(j)} \right\|_{\infty} + c_1 + \tilde{A}c_2.$$

Lemma 1 shows that PairBalance reduces the parallel herding objective (8) towards a constant (invariant to n) at each step. This implies that, if we repeatedly call PairBalance on a given permutation, it will return a permutation that guarantees the parallel herding bound to be $\tilde{O}(1)$.

Proof. We prove this lemma by defining the following auxiliary sequence,

$$\mathbf{y}_{n \cdot (k-1) + i} = \mathbf{z}_{i, \pi_i(2k-1)} - \mathbf{z}_{i, \pi_i(2k)}, \quad \forall k \in [n/2],$$

which we also can refer to as $\{\mathbf{y}_j\}_{j=1}^{mn/2}$.

We also leverage Statement 1, which we reprint below for clarity of presentation:

Statement 1. For the RandomizedBalance subroutine in Algorithm 2 [2], there exists a constant $\tilde{A} = \tilde{O}(1)$ such that for any input vectors $\{\mathbf{z}_j\}_{j=1}^N$ with $\|\mathbf{z}_j\|_2 \leq 1$, RandomizedBalance outputs a sequence of signs $\{s_j\}_{j=1}^N \in \{-1, 1\}$ that fulfill $\max_{k \in [N]} \left\| \sum_{j=1}^k s_j (\mathbf{z}_j - \bar{\mathbf{z}}) \right\|_{\infty} \leq \tilde{A}$, with $\bar{\mathbf{z}} = \frac{1}{N} \sum_{i=1}^N \mathbf{z}_i$.

Note that the reordering part of Algorithm 7 (line 8) gives a sequence of signs $\{s_j\}_{j=1}^{mn/2}$. Therefore, by the above statement, the sequence $\{\mathbf{y}_j\}_{j=1}^{mn/2}$ satisfies

$$\max_{P \in [mn/2]} \left\| \sum_{p=1}^P s_p \mathbf{y}_p \right\|_{\infty} \leq 2\tilde{A}c_2, \quad (9)$$

since

$$\|\mathbf{y}_{n(k-1)+i}\|_{\infty} \leq \left\| \mathbf{z}_{i, \pi_{t,i}(2k-1)} - \frac{1}{mn} \sum_{i=1}^m \sum_{j=1}^n \mathbf{z}_{i,j} \right\|_{\infty} + \left\| \mathbf{z}_{i, \pi_{t,i}(2k)} - \frac{1}{mn} \sum_{i=1}^m \sum_{j=1}^n \mathbf{z}_{i,j} \right\|_{\infty} \leq 2c_2.$$

Note that, if $s_{i,k}$ is the sign associated with $\mathbf{y}_{n(k-1)+i}$, then $\mathbf{z}_{i, \pi_{t,i}(2k-1)}$ and $\mathbf{z}_{i, \pi_{t,i}(2k)}$ will receive opposite signs $s_{i,k}$ and $-s_{i,k}$, respectively.

We denote $\mathbf{x}_{i,k}^+$ to be the term that receives $s_{i,k} = +1$ and $\mathbf{x}_{i,k}^-$ to be the term that receives $s_{i,k} = -1$.

That is: If $s_{i,k} = +1$, then $\mathbf{x}_{i,k}^+ = \mathbf{z}_{i, \pi_i(2k-1)}$, otherwise, if $s_{i,k} = -1$, then $\mathbf{x}_{i,k}^+ = \mathbf{z}_{i, \pi_i(2k)}$; and, $\mathbf{x}_{i,k}^-$ is the other term of the pair $\{\mathbf{z}_{i, \pi_i(2k-1)}, \mathbf{z}_{i, \pi_i(2k)}\}$.

Now, for $K \in [\frac{n}{2}]$, let

$$\begin{aligned} \kappa_{i,K} &= \sum_{k=1}^K (\mathbf{z}_{i, \pi_i(2k-1)} + \mathbf{z}_{i, \pi_i(2k)}), \\ v_{i,K} &= \sum_{k=1}^K (s_{i,k} \mathbf{z}_{i, \pi_i(2k-1)} - s_{i,k} \mathbf{z}_{i, \pi_i(2k)}). \end{aligned}$$

Then

$$\begin{aligned} \sum_{k=1}^K \mathbf{x}_{i,k}^+ &= \frac{1}{2} (\kappa_{i,K} + v_{i,K}) \quad \text{and} \\ \sum_{k=1}^K \mathbf{x}_{i,k}^- &= \frac{1}{2} (\kappa_{i,K} - v_{i,K}). \end{aligned}$$

Now, observe that

$$\begin{aligned}\sum_{i=1}^m \kappa_{i,K} &= \sum_{j=1}^{2K} \sum_{i=1}^m \mathbf{z}_{i,\pi_i(j)} \quad \text{and} \\ \sum_{i=1}^m v_{i,K} &= \sum_{p=1}^{mK} s_p \mathbf{y}_p.\end{aligned}$$

Therefore:

$$\begin{aligned}\max_{K \in [n/2]} \left\| \sum_{k=1}^K \sum_{i=1}^m \mathbf{x}_{i,k}^+ \right\|_{\infty} &\leq \frac{1}{2} \left(\max_{K \in [n/2]} \left\| \sum_{i=1}^m \kappa_{K,i} \right\|_{\infty} + \max_{K \in [n/2]} \left\| \sum_{i=1}^m v_{K,i} \right\|_{\infty} \right) \\ &\leq \frac{1}{2} \max_{K \in [n/2]} \left\| \sum_{j=1}^{2K} \sum_{i=1}^m \mathbf{z}_{i,j} \right\|_{\infty} + \tilde{A}c_2 \quad \text{By substituting above and (9)} \\ &\leq \frac{1}{2} \max_{k \in [n]} \left\| \sum_{j=1}^k \sum_{i=1}^m \mathbf{z}_{i,j} \right\|_{\infty} + \tilde{A}c_2.\end{aligned}$$

And similarly:

$$\begin{aligned}\max_{K \in [n/2]} \left\| \sum_{k=1}^K \sum_{i=1}^m \mathbf{x}_{i,k}^- \right\|_{\infty} &\leq \frac{1}{2} \left(\max_{K \in [n/2]} \left\| \sum_{i=1}^m \kappa_{K,i} \right\|_{\infty} + \max_{K \in [n/2]} \left\| \sum_{i=1}^m v_{K,i} \right\|_{\infty} \right) \\ &\leq \frac{1}{2} \max_{k \in [n]} \left\| \sum_{j=1}^k \sum_{i=1}^m \mathbf{z}_{i,j} \right\|_{\infty} + \tilde{A}c_2.\end{aligned}$$

Applying the permutation $\pi'_i(j)$ on the vectors $\mathbf{z}_{i,\pi_i(j)}$, we get for each $i \in [m]$ the permuted sequence

$$\mathbf{x}_{i,1}^+, \dots, \mathbf{x}_{i,n/2}^+, \mathbf{x}_{i,n/2}^-, \dots, \mathbf{x}_{i,1}^-,$$

and thus we need to bound the herding objective of the sequence

$$\sum_{i=1}^m \mathbf{x}_{i,1}^+, \dots, \sum_{i=1}^m \mathbf{x}_{i,n/2}^+, \sum_{i=1}^m \mathbf{x}_{i,n/2}^-, \dots, \sum_{i=1}^m \mathbf{x}_{i,1}^-.$$

If the partial sums above peak at $t_0 \leq n/2$, then we can bound the parallel herding objective as:

$$\left\| \sum_{k=1}^{t_0} \sum_{i=1}^m \mathbf{x}_{i,k}^+ \right\|_{\infty} = \max_{K \in [n/2]} \left\| \sum_{k=1}^K \sum_{i=1}^m \mathbf{x}_{i,k}^+ \right\|_{\infty} \leq \frac{1}{2} \max_{k \in [n]} \left\| \sum_{j=1}^k \sum_{i=1}^m \mathbf{z}_{i,j} \right\|_{\infty} + \tilde{A}c_2;$$

else, we can bound the parallel herding objective as:

$$\begin{aligned}\left\| \sum_{j=1}^n \sum_{i=1}^m \mathbf{z}_{i,j} - \sum_{k=1}^{m-t_0} \sum_{i=1}^m \mathbf{x}_{i,k}^- \right\|_{\infty} &\leq \left\| \sum_{j=1}^n \sum_{i=1}^m \mathbf{z}_{i,j} \right\|_{\infty} + \left\| \sum_{k=1}^{m-t_0} \sum_{i=1}^m \mathbf{x}_{i,k}^- \right\|_{\infty} \\ &\leq c_1 + \frac{1}{2} \max_{t \in [n]} \left\| \sum_{j=1}^t \sum_{i=1}^m \mathbf{z}_{i,j} \right\|_{\infty} + \tilde{A}c_2,\end{aligned}$$

since in Algorithm 1 the list of vectors with negative signs is reversed before concatenated.

The claim follows. \square

C.2 Additional Lemmas

Recall that one t -th step of the parameter update can be written as:

$$\mathbf{w}_t^{j+1} = \mathbf{w}_t^j - \frac{\alpha}{m} \sum_{i=1}^m \nabla f^i(\mathbf{w}_t^j; \pi_{t,i}(j)), \quad \forall j \in [n]$$

We will use the convention $\mathbf{w}_{t+1} \triangleq \mathbf{w}_{t+1}^1 \triangleq \mathbf{w}_t^{n+1}$. The key quantity in our proof is Δ_t , defined as:

$$\begin{aligned} \Delta_t &\triangleq \max_{k \in [n]} \|\mathbf{w}_t^{k+1} - \mathbf{w}_t\|_\infty \\ &= \frac{\alpha}{m} \max_{k \in [n]} \left\| \sum_{j=1}^k \sum_{i=1}^m \nabla f^i(\mathbf{w}_t^j, \pi_{t,i}(j)) \right\|_\infty. \end{aligned}$$

We also make repeated use of the following observation:

$$\begin{aligned} \|\mathbf{w}_t^j - \mathbf{w}_t^k\|_\infty &\leq \|\mathbf{w}_t^j - \mathbf{w}_t\|_\infty + \|\mathbf{w}_t^k - \mathbf{w}_t\|_\infty \leq 2\Delta_t \\ \|\mathbf{w}_{t+1}^j - \mathbf{w}_t^k\|_\infty &\leq \|\mathbf{w}_{t+1}^j - \mathbf{w}_{t+1}\|_\infty + \|\mathbf{w}_{t+1} - \mathbf{w}_t\|_\infty + \|\mathbf{w}_t^k - \mathbf{w}_t\|_\infty \leq \Delta_{t+1} + 2\Delta_t, \end{aligned}$$

for all $j, k \in [n]$. This relation is mostly used in combination with the Lipschitz assumptions to bound gradients of the same loss function but with different parameters. We also denote $F_t = f(\mathbf{w}_t) - f(\mathbf{w}^*)$ where \mathbf{w}^* is the minimizer of f which we assume to be bounded from below.

Lemma 2. 1. If the learning rate $\alpha \leq \frac{1}{nL}$ then:

$$\frac{1}{T} \sum_{t=1}^T \|\nabla f(\mathbf{w}_t)\|_2^2 \leq \frac{2\delta_0}{\alpha n T} + \frac{L_{2,\infty}^2}{T} \sum_{t=1}^T \Delta_t^2,$$

2. If, further, the PL assumption holds then, for $\rho = 1 - \frac{\alpha n \mu}{2}$:

$$F_{T+1} \leq \rho^T F_1 + \frac{\alpha n L_{2,\infty}^2}{2} \sum_{t=1}^T \rho^{T-t} \left(\Delta_t^2 - \frac{1}{2L_{2,\infty}^2} \|f(\mathbf{w}_t)\|_2^2 \right).$$

Proof. Using the definition of L -smoothness:

$$f(\mathbf{w}_{t+1}) \leq f(\mathbf{w}_t) + \nabla f(\mathbf{w}_t)^\top (\mathbf{w}_{t+1} - \mathbf{w}_t) + (L/2) \|\mathbf{w}_{t+1} - \mathbf{w}_t\|_2^2$$

and

$$\begin{aligned} -\nabla f(\mathbf{w}_t)^\top (\mathbf{w}_t - \mathbf{w}_{t+1}) &= -\frac{\alpha n}{2} 2 \nabla f(\mathbf{w}_t)^\top \left(\frac{\mathbf{w}_t - \mathbf{w}_{t+1}}{\alpha n} \right) \\ &= \frac{\alpha n}{2} \left(\left\| \nabla f(\mathbf{w}_t) - \frac{(\mathbf{w}_t - \mathbf{w}_{t+1})}{\alpha n} \right\|_2^2 - \|\nabla f(\mathbf{w}_t)\|_2^2 - \left\| \frac{(\mathbf{w}_t - \mathbf{w}_{t+1})}{\alpha n} \right\|_2^2 \right), \end{aligned}$$

we get

$$\begin{aligned} f(\mathbf{w}_{t+1}) &\leq f(\mathbf{w}_t) + \frac{\alpha n}{2} \left\| \nabla f(\mathbf{w}_t) - \frac{(\mathbf{w}_t - \mathbf{w}_{t+1})}{\alpha n} \right\|_2^2 - \frac{\alpha n}{2} \|\nabla f(\mathbf{w}_t)\|_2^2 \\ &\quad + \frac{\alpha n L - 1}{2\alpha n} \|\mathbf{w}_t - \mathbf{w}_{t+1}\|_2^2. \end{aligned}$$

The last term on the RHS is ≤ 0 by assumption $\alpha \leq \frac{1}{nL}$, therefore

$$f(\mathbf{w}_{t+1}) \leq f(\mathbf{w}_t) + \frac{\alpha n}{2} \left\| \nabla f(\mathbf{w}_t) - \frac{(\mathbf{w}_t - \mathbf{w}_{t+1})}{\alpha n} \right\|_2^2 - \frac{\alpha n}{2} \|\nabla f(\mathbf{w}_t)\|_2^2.$$

We next bound the second term on the RHS by the discrepancy Δ_t :

$$\begin{aligned} \left\| \nabla f(\mathbf{w}_t) - \frac{(\mathbf{w}_t - \mathbf{w}_{t+1})}{\alpha n} \right\|_2^2 &= \left\| \frac{1}{mn} \sum_{j=1}^m \sum_{i=1}^n \nabla f^i(\mathbf{w}_t, \pi_t(j)) - \frac{1}{mn} \sum_{j=1}^m \sum_{i=1}^n \nabla f^i(\mathbf{w}_t^j; \pi_t(j)) \right\|_2^2 \\ &\leq \frac{1}{mn} \sum_{j=1}^m \sum_{i=1}^n \left\| \nabla f^i(\mathbf{w}_t, \pi_t(j)) - \nabla f^i(\mathbf{w}_t^j; \pi_t(j)) \right\|_2^2 \\ &\leq \frac{L_{2,\infty}^2}{mn} \sum_{j=1}^m \sum_{i=1}^n \left\| \mathbf{w}_t^j - \mathbf{w}_t \right\|_\infty^2 \\ &\leq L_{2,\infty}^2 \Delta_t^2 \end{aligned}$$

where we have used the $L_{2,\infty}$ -smoothness assumption 3 in the second-to-last inequality. Plug this bound back:

$$f(\mathbf{w}_{t+1}) \leq f(\mathbf{w}_t) + \frac{\alpha n L_{2,\infty}^2}{2} \Delta_t^2 - \frac{\alpha n}{2} \|\nabla f(\mathbf{w}_t)\|_2^2 \quad (10)$$

For part (1), we average 10 over $t \in [T]$ to get:

$$\begin{aligned} \frac{1}{T} \sum_{t=1}^T \|\nabla f(\mathbf{w}_t)\|_2^2 &\leq \frac{2(f(\mathbf{w}_1) - f(\mathbf{w}_{T+1}))}{\alpha n T} + \frac{L_{2,\infty}^2}{T} \sum_{t=1}^T \Delta_t^2 \\ &\leq \frac{2F_1}{\alpha n T} + \frac{L_{2,\infty}^2}{T} \sum_{t=1}^T \Delta_t^2. \end{aligned}$$

For part (2), we use the PL condition on 10 to get:

$$\begin{aligned} f(\mathbf{w}_{t+1}) &\leq f(\mathbf{w}_t) + \frac{\alpha n L_{2,\infty}^2}{2} \Delta_t^2 - \frac{\alpha n}{4} \|\nabla f(\mathbf{w}_t)\|_2^2 - \frac{\alpha n}{4} \|f(\mathbf{w}_t)\|_2^2 \\ &\leq f(\mathbf{w}_t) + \frac{\alpha n L_{2,\infty}^2}{2} \Delta_t^2 - \frac{\alpha n \mu}{2} (f(\mathbf{w}_t) - f(\mathbf{w}^*)) - \frac{\alpha n}{4} \|f(\mathbf{w}_t)\|_2^2, \end{aligned}$$

then subtract both sides by f^* :

$$f(\mathbf{w}_{t+1}) - f^* \leq \left(1 - \frac{\alpha n \mu}{2}\right) (f(\mathbf{w}_t) - f^*) + \frac{\alpha n}{2} \left(L_{2,\infty}^2 \Delta_t^2 - \frac{1}{2} \|f(\mathbf{w}_t)\|_2^2 \right),$$

and apply the above inequality recursively for $t \in [T]$:

$$F_{T+1} \leq \rho^T F_1 + \frac{\alpha n L_{2,\infty}^2}{2} \sum_{t=1}^T \rho^{T-t} \left(\Delta_t^2 - \frac{1}{2L_{2,\infty}^2} \|f(\mathbf{w}_t)\|_2^2 \right),$$

for $\rho = 1 - \frac{\alpha n \mu}{2}$. □

Lemma 3. For $t \in [T]$, if we apply Algorithm 7 to the gradients $\nabla f^i(\mathbf{w}_t^j, \pi_t^i(j))$ at epoch t to produce the next permutation $\pi_{t+1,i}$ for epoch $t+1$, then:

$$\begin{aligned} \Delta_{t+1} &\leq \frac{1}{2}\Delta_t + \alpha L_\infty \left(4n + \frac{2\tilde{A}}{m}\right) \Delta_t + \alpha n L_\infty \Delta_{t+1} \\ &\quad + \frac{\alpha(\varsigma + \sigma)\tilde{A}}{m} + \alpha n \|\nabla f(\mathbf{w}_{t+1})\|_2 \end{aligned}$$

Proof. We start with the triangle inequality:

$$\begin{aligned} \left\| \sum_{j=1}^k \sum_{i=1}^m \nabla f^i(\mathbf{w}_{t+1}^j, \pi_{t+1,i}(j)) \right\|_\infty &\leq \left\| \sum_{j=1}^k \sum_{i=1}^m \nabla f^i(\mathbf{w}_t^{\pi_{t,i}^{-1}\pi_{t+1,i}(j)}, \pi_{t+1,i}(j)) \right\|_\infty + \\ &\quad \left\| \sum_{j=1}^k \sum_{i=1}^m \left(\nabla f^i(\mathbf{w}_{t+1}^j, \pi_{t+1,i}(j)) - \nabla f^i(\mathbf{w}_t^{\pi_{t,i}^{-1}\pi_{t+1,i}(j)}, \pi_{t+1,i}(j)) \right) \right\|_\infty \end{aligned} \quad (11)$$

We use lemma 1 to bound the first term on the RHS of 11. Let:

$$\mathbf{z}_{i,j} = \nabla f^i(\mathbf{w}_t^{\pi_{t,i}^{-1}(j)}; j),$$

so that:

$$\mathbf{z}_{i,\pi_{t+1,i}(j)} = \nabla f^i(\mathbf{w}_t^{\pi_{t,i}^{-1}\pi_{t+1,i}(j)}; \pi_{t+1,i}(j)).$$

The upper bounds for $\left\| \mathbf{z}_{i,j} - \frac{1}{mn} \sum_{r,s} \mathbf{z}_{r,s} \right\|_\infty$ and $\left\| \sum_{i,j} \mathbf{z}_{i,j} \right\|_\infty$ are:

$$\left\| \nabla f^i(\mathbf{w}_t^j; \pi_{t,i}(j)) - \frac{1}{mn} \sum_{r=1}^m \sum_{s=1}^n \nabla f^s(\mathbf{w}_t^r; \pi_{t,s}(r)) \right\|_\infty,$$

which are

$$\begin{aligned} &\leq \left\| \nabla f^i(\mathbf{w}_t^j; \pi_{t,i}(j)) - \frac{1}{mn} \sum_{r=1}^m \sum_{s=1}^n \nabla f^s(\mathbf{w}_t^j; \pi_{t,s}(r)) \right\|_\infty + \\ &\quad \left\| \frac{1}{mn} \sum_{r=1}^m \sum_{s=1}^n \nabla f^s(\mathbf{w}_t^j; \pi_{t,s}(r)) - \frac{1}{mn} \sum_{r=1}^m \sum_{s=1}^n \nabla f^s(\mathbf{w}_t^r; \pi_{t,s}(r)) \right\|_\infty. \end{aligned}$$

We can rewrite the above to be

$$\begin{aligned} &\leq \left\| \nabla f^i(\mathbf{w}_t^j; \pi_{t,i}(j)) - \nabla f(\mathbf{w}_t^j) \right\|_\infty + \frac{L_\infty}{mn} \sum_{r=1}^m m \sum_{s=1}^n \left\| \mathbf{w}_t^j - \mathbf{w}_t^r \right\|_\infty \\ &\leq \varsigma + \sigma + 2L_\infty \Delta_t. \end{aligned}$$

Now, observe that

$$\begin{aligned} \left\| \sum_{i=1}^m \sum_{j=1}^n \nabla f^i(\mathbf{w}_t^j; \pi_{t,i}(j)) \right\|_\infty &\leq \left\| \sum_{i=1}^m \sum_{j=1}^n \nabla f^i(\mathbf{w}_t^j; \pi_{t,i}(j)) - \sum_{i=1}^m \sum_{j=1}^n \nabla f^i(\mathbf{w}_{t+1}; \pi_{t,i}(j)) \right\|_\infty + \\ &\quad \left\| \sum_{i=1}^m \sum_{j=1}^n \nabla f^i(\mathbf{w}_{t+1}; \pi_{t,i}(j)) \right\|_\infty. \end{aligned}$$

We can rewrite the RHS to be

$$\begin{aligned} &\leq \sum_{i=1}^m \sum_{j=1}^n L_\infty \left\| \mathbf{w}_t^j - \mathbf{w}_{t+1} \right\|_\infty + mn \|\nabla f(\mathbf{w}_{t+1})\|_\infty \\ &\leq 2mnL_\infty \Delta_t + mn \|\nabla f(\mathbf{w}_{t+1})\|_2, \end{aligned}$$

by using the above. Therefore, by lemma 1:

$$\begin{aligned} \max_{k \in [n]} \left\| \sum_{j=1}^k \sum_{i=1}^m \nabla f^i(\mathbf{w}_t^{\pi_{t,i}^{-1} \pi_{t+1,i}(j)}, \pi_{t+1,i}(j)) \right\|_\infty &\leq \max_{k \in [n]} \left\| \sum_{j=1}^k \sum_{i=1}^m \nabla f^i(\mathbf{w}_t^j, \pi_{t,i}(j)) \right\|_\infty \\ &\quad + 2mnL_\infty \Delta_t + \|\nabla f(\mathbf{w}_{t+1})\|_2 + (\varsigma + \sigma + 2L_\infty \Delta_t) \tilde{A}. \end{aligned}$$

The second term of 11 can be bounded as:

$$\left\| \sum_{j=1}^k \sum_{i=1}^m \left(\nabla f^i(\mathbf{w}_{t+1,i}^j; \pi_{t+1,i}(j)) - \nabla f^i(\mathbf{w}_{t,i}^{\pi_{t,i}^{-1} \pi_{t+1,i}(j)}; \pi_{t+1,i}(j)) \right) \right\|_\infty,$$

which is

$$\begin{aligned} &\leq \sum_{j=1}^k \sum_{i=1}^m \left\| \mathbf{w}_{t+1,i}^j - \mathbf{w}_{t,i}^{\pi_{t,i}^{-1} \pi_{t+1,i}(j)} \right\|_\infty \\ &\leq mnL_\infty (\Delta_{t+1} + 2\Delta_t). \end{aligned}$$

Substitute these bounds into the RHS of 11, take the max of both sides and group terms, we get:

$$\begin{aligned} \max_{k \in [n]} \left\| \sum_{j=1}^k \sum_{i=1}^m \nabla f^i(\mathbf{w}_{t+1,i}^j, \pi_{t+1,i}(j)) \right\|_\infty &\leq \frac{1}{2} \max_{k \in [n]} \left\| \sum_{j=1}^k \sum_{i=1}^m \nabla f^i(\mathbf{w}_t^j, \pi_{t,i}(j)) \right\|_\infty \\ &\quad + L_\infty (4mn + 2\tilde{A}) \Delta_t + mnL_\infty \Delta_{t+1} + (\varsigma + \sigma) \tilde{A} \\ &\quad + mn \|\nabla f(\mathbf{w}_{t+1})\|_2. \end{aligned}$$

Multiply both sides by $\frac{\alpha}{m}$ and use the definition of Δ_t , we get the claim. \square

Lemma 4. 1. If the learning rate $\alpha \leq \frac{1}{16 \max\{L_\infty, L_{2,\infty}\}(2n+\tilde{A}/m)}$ then:

$$\frac{1}{T} \sum_{t=1}^T \Delta_t^2 \leq \frac{21\alpha^2(\zeta+\sigma)^2\tilde{A}^2}{m^2} + \frac{9\alpha^2n^2\sigma^2}{T} + 21\alpha^2n^2\frac{1}{T} \sum_{t=1}^T \|\nabla f(\mathbf{w}_t)\|_2^2.$$

2. If further $\alpha \leq \frac{2}{9n\mu}$, then, for $\rho = 1 - \frac{\alpha n\mu}{2}$:

$$\sum_{t=1}^T \rho^{T-t} \Delta_t^2 \leq 12\rho^{T-1}\alpha^2n^2\sigma^2 + \frac{28\rho\alpha^2(\zeta+\sigma)^2\tilde{A}^2}{(1-\rho)m^2} + \frac{1}{2L_{2,\infty}^2} \sum_{t=1}^T \rho^{T-t} \|\nabla f(\mathbf{w}_t)\|_2^2.$$

Proof. First we bound Δ_1^2 . We start with a series of triangle inequalities:

$$\begin{aligned} \frac{\alpha}{m} \left\| \sum_{j=1}^k \sum_{i=1}^m \nabla f^i(\mathbf{w}_1^j, \pi_{1,i}(j)) \right\|_\infty &\leq \frac{\alpha}{m} \left\| \sum_{j=1}^k \sum_{i=1}^m \nabla f^i(\mathbf{w}_1^j, \pi_{1,i}(j)) - \sum_{j=1}^k \sum_{i=1}^m \nabla f^i(\mathbf{w}_1, \pi_{1,i}(j)) \right\|_\infty \\ &\quad + \frac{\alpha}{m} \left\| \sum_{j=1}^k \sum_{i=1}^m (\nabla f^i(\mathbf{w}_1, \pi_{1,i}(j)) - \nabla f^i(\mathbf{w}_1)) \right\|_\infty + \alpha k \|\nabla f(\mathbf{w}_1)\|_\infty \\ &\leq \frac{\alpha}{m} \sum_{j=1}^k \sum_{i=1}^m L_\infty \|\mathbf{w}_1^j - \mathbf{w}_1\|_\infty + \alpha k \sigma + \alpha k \|\nabla f(\mathbf{w}_1)\|_2, \end{aligned}$$

so that after taking the max of both sides w.r.t. $k \in [n]$:

$$\begin{aligned} \Delta_1 &\leq \alpha n L_\infty \Delta_1 + \alpha n \sigma + \alpha n \|\nabla f(\mathbf{w}_1)\|_2 \\ &\leq (1/32)\Delta_1 + \alpha n \sigma + \alpha n \|\nabla f(\mathbf{w}_1)\|_2 \\ &\leq (32/31)\alpha n \sigma + (32/31)\alpha n \|\nabla f(\mathbf{w}_1)\|_2, \end{aligned}$$

where we have used $\alpha \leq \frac{1}{32nL_\infty}$. Square both sides:

$$\Delta_1^2 \leq 3\alpha^2n^2\sigma^2 + 3\alpha^2n^2\|\nabla f(\mathbf{w}_1)\|_2^2. \quad (12)$$

Now we use lemma 3 to get the relationship between Δ_{t+1} and Δ_t for $t \in [T]$. Recall that:

$$\begin{aligned} \Delta_{t+1} &\leq \frac{1}{2}\Delta_t + \alpha L_\infty \left(4n + \frac{2\tilde{A}}{m} \right) \Delta_t + \alpha n L_\infty \Delta_{t+1} + \frac{\alpha(\zeta+\sigma)\tilde{A}}{m} + \alpha n \|\nabla f(\mathbf{w}_{t+1})\|_2 \\ &\leq \frac{1}{2}\Delta_t + (1/8)\Delta_t + (1/32)\Delta_{t+1} + \frac{\alpha(\zeta+\sigma)\tilde{A}}{m} + \alpha n \|\nabla f(\mathbf{w}_{t+1})\|_2, \end{aligned}$$

due to $\alpha \leq \frac{1}{16L_\infty(2n+\tilde{A}/m)}$. Square both sides:

$$\begin{aligned} (31/32)^2 \Delta_{t+1}^2 &\leq \frac{1}{2}\Delta_t^2 + 2 \left((1/8)\Delta_t + \frac{\alpha(\zeta+\sigma)\tilde{A}}{m} + \alpha n \|\nabla f(\mathbf{w}_{t+1})\|_2 \right)^2 \\ &\leq \frac{1}{2}\Delta_t^2 + (6/8^2)\Delta_t^2 + \frac{6\alpha^2(\zeta+\sigma)^2\tilde{A}^2}{m^2} + 6\alpha^2n^2\|\nabla f(\mathbf{w}_{t+1})\|_2^2, \end{aligned}$$

so that

$$\begin{aligned} \Delta_{t+1}^2 &\leq (32/31)^2(1/2 + 6/8^2)\Delta_t^2 + \frac{(32/31)^2 6\alpha^2(\zeta+\sigma)^2\tilde{A}^2}{m^2} + (32/31)^2 6\alpha^2n^2\|\nabla f(\mathbf{w}_{t+1})\|_2^2 \\ &\leq (2/3)\Delta_t^2 + \frac{7\alpha^2(\zeta+\sigma)^2\tilde{A}^2}{m^2} + 7\alpha^2n^2\|\nabla f(\mathbf{w}_{t+1})\|_2^2. \end{aligned} \quad (13)$$

For part (1), we sum 13 over $t \in [T-1]$ and add 12:

$$\begin{aligned}\Delta_1^2 + \sum_{t=2}^T \Delta_t^2 &\leq (2/3) \sum_{t=2}^T \Delta_{t-1}^2 + \frac{(T-1)7\alpha^2(\varsigma+\sigma)^2\tilde{A}^2}{m^2} + 3\alpha^2n^2\sigma^2 + 7\alpha^2n^2 \sum_{t=1}^T \|\nabla f(\mathbf{w}_t)\|_2^2 \\ \frac{1}{T} \sum_{t=1}^T \Delta_t^2 &\leq (2/3) \frac{1}{T} \sum_{t=1}^T \Delta_t^2 + \frac{7\alpha^2(\varsigma+\sigma)^2\tilde{A}^2}{m^2} + \frac{3\alpha^2n^2\sigma^2}{T} + 7\alpha^2n^2 \frac{1}{T} \sum_{t=1}^T \|\nabla f(\mathbf{w}_t)\|_2^2 \\ &\leq \frac{21\alpha^2(\varsigma+\sigma)^2\tilde{A}^2}{m^2} + \frac{9\alpha^2n^2\sigma^2}{T} + 21\alpha^2n^2 \frac{1}{T} \sum_{t=1}^T \|\nabla f(\mathbf{w}_t)\|_2^2.\end{aligned}$$

For part (2), we multiply each term Δ_t with ρ^{T-t} for $t \in [T]$ and use the bounds 12 and 13:

$$\begin{aligned}\rho^{T-1}\Delta_1^2 &\leq \rho^{T-1}3\alpha^2n^2\sigma^2 + \rho^{T-1}3\alpha^2n^2\|\nabla f(\mathbf{w}_1)\|_2^2 \\ \rho^{T-t}\Delta_t^2 &\leq (2/3)\rho^{T-t}\Delta_{t-1}^2 + \rho^{T-t}\frac{7\alpha^2(\varsigma+\sigma)^2\tilde{A}^2}{m^2} + \rho^{T-t}7\alpha^2n^2\|\nabla f(\mathbf{w}_t)\|_2^2 \\ &\leq (3/4)\rho^{T-(t-1)}\Delta_{t-1}^2 + \rho^{T-t}\frac{7\alpha^2(\varsigma+\sigma)^2\tilde{A}^2}{m^2} + \rho^{T-t}7\alpha^2n^2\|\nabla f(\mathbf{w}_t)\|_2^2, \quad \forall t \in \{2, \dots, T\}\end{aligned}$$

where we have used $\alpha \leq \frac{2}{9n\mu}$ so that $\rho = 1 - (1/2)\alpha n\mu \geq (2/3)(4/3)$. Now sum the previous bounds for $\rho^{T-t}\Delta_t$ for all $t \in [T]$ we get:

$$\begin{aligned}\rho^{T-1}\Delta_1^2 + \sum_{t=2}^T \rho^{T-t}\Delta_t^2 &\leq \frac{3}{4} \sum_{t=2}^T \rho^{T-(t-1)}\Delta_{t-1}^2 + \rho^{T-1}3\alpha^2n^2\sigma^2 + \sum_{t=1}^T \rho^{T-t}\frac{7\alpha^2(\varsigma+\sigma)^2\tilde{A}^2}{m^2} + \\ &\quad 7\alpha^2n^2 \sum_{t=1}^T \rho^{T-t}\|\nabla f(\mathbf{w}_t)\|_2^2.\end{aligned}$$

We can rewrite the RHS as

$$\begin{aligned}&\leq \frac{3}{4} \sum_{t=1}^T \rho^{T-t}\Delta_t^2 + \rho^{T-1}3\alpha^2n^2\sigma^2 + \frac{7\rho\alpha^2(\varsigma+\sigma)^2\tilde{A}^2}{(1-\rho)m^2} + 7\alpha^2n^2 \sum_{t=1}^T \rho^{T-t}\|\nabla f(\mathbf{w}_t)\|_2^2 \\ &\leq 12\rho^{T-1}\alpha^2n^2\sigma^2 + \frac{28\rho\alpha^2(\varsigma+\sigma)^2\tilde{A}^2}{(1-\rho)m^2} + 28\alpha^2n^2 \sum_{t=1}^T \rho^{T-t}\|\nabla f(\mathbf{w}_t)\|_2^2.\end{aligned}$$

Lastly, we use $\alpha \leq \frac{1}{\sqrt{56n}L_{2,\infty}}$ to get:

$$\sum_{t=1}^T \rho^{T-t}\Delta_t^2 \leq 12\rho^{T-1}\alpha^2n^2\sigma^2 + \frac{28\rho\alpha^2(\varsigma+\sigma)^2\tilde{A}^2}{(1-\rho)m^2} + \frac{1}{2L_{2,\infty}^2} \sum_{t=1}^T \rho^{T-t}\|\nabla f(\mathbf{w}_t)\|_2^2.$$

□

C.3 Proof of Theorems 1 and 2

Using the lemmas above, we next prove our main results, presented in Section 4.

Proof of theorem 1. The given learning rate α satisfies the constraints of part 1 of lemma 2 and lemma 4, so we get:

$$\begin{aligned} \frac{1}{T} \sum_{t=1}^T \|\nabla f(\mathbf{w}_t)\|_2^2 &\leq \frac{2F_1}{\alpha n T} + L_{2,\infty}^2 \left(\frac{21(\alpha(\varsigma + \sigma)\tilde{A})^2}{m^2} + \frac{9(\alpha n \sigma)^2}{T} + 21\alpha^2 n^2 \frac{1}{T} \sum_{t=1}^T \|\nabla f(\mathbf{w}_t)\|_2^2 \right) \\ &\leq \frac{4F_1}{\alpha n T} + \frac{42L_{2,\infty}^2(\alpha(\varsigma + \sigma)\tilde{A})^2}{m^2} + \frac{18L_{2,\infty}^2(\alpha n \sigma)^2}{T}, \end{aligned}$$

due to $\alpha \leq \frac{1}{\sqrt{42n}L_{2,\infty}}$. We next derive the convergence rate. Let $\Gamma = \frac{42(L_{2,\infty}(\varsigma + \sigma)\tilde{A})^2}{m^2} + \frac{18L_{2,\infty}^2 n^2 \sigma^2}{T}$ then:

$$\frac{1}{T} \sum_{t=1}^T \|\nabla f(\mathbf{w}_t)\|_2^2 \leq \frac{4F_1}{\alpha n T} + \Gamma \alpha^2.$$

We then set $\alpha \leq \left(\frac{4F_1}{n\Gamma T}\right)^{1/3}$. So we will have $\alpha = \min \left\{ \frac{1}{16 \max\{L_\infty, L_{2,\infty}\}(2n + \tilde{A}/m)}, \left(\frac{4F_1}{n\Gamma T}\right)^{1/3} \right\}$ or

$$\frac{1}{a} = \max \left\{ 16 \max\{L_\infty, L_{2,\infty}\}(2n + \tilde{A}/m), \left(\frac{4F_1}{n\Gamma T}\right)^{-1/3} \right\}.$$

Substitute α :

$$\begin{aligned} \frac{1}{T} \sum_{t=1}^T \|\nabla f(\mathbf{w}_t)\|_2^2 &\leq \frac{4F_1}{nT} \left\{ 16 \max\{L_\infty, L_{2,\infty}\}(2n + \tilde{A}/m) + \left(\frac{4F_1}{n\Gamma T}\right)^{-1/3} \right\} + \Gamma \left(\frac{4F_1}{n\Gamma T}\right)^{2/3} \\ &\leq \left(\frac{4F_1}{nT}\right)^{2/3} \Gamma^{1/3} + \frac{64F_1 \max\{L_\infty, L_{2,\infty}\}(2 + \tilde{A}/(mn))}{T} \\ &\leq \left(\frac{4F_1}{nT}\right)^{2/3} \left(\frac{(\sqrt{42}L_{2,\infty}(\varsigma + \sigma)\tilde{A})^{2/3}}{m^{2/3}} + \frac{(\sqrt{18}L_{2,\infty}n\sigma)^{2/3}}{T^{1/3}} \right) \\ &\quad + \frac{64F_1 \max\{L_\infty, L_{2,\infty}\}(2 + \tilde{A}/(mn))}{T} \\ &\leq \frac{(4\sqrt{42}F_1 L_{2,\infty}(\varsigma + \sigma)\tilde{A})^{2/3}}{(mnT)^{2/3}} + \frac{(72F_1 L_{2,\infty}\sigma)^{2/3}}{T} \\ &\quad + \frac{64F_1 \max\{L_\infty, L_{2,\infty}\}(2 + \tilde{A}/(mn))}{T}, \end{aligned}$$

in which the leading term (slowest in terms of T) is $\tilde{O}((mnT)^{-2/3})$, proving the claim. \square

Proof of theorem 2. With the P.L. assumption 4, we use part 2 of lemma 2 and lemma 4 (we show that their

constraints are satisfied later) to get:

$$\begin{aligned}
F_{T+1} &\leq \rho^T F_1 + \frac{\alpha n L_{2,\infty}^2}{2} \sum_{t=1}^T \rho^{T-t} \left(\Delta_t^2 - \frac{1}{2L_{2,\infty}^2} \|f(\mathbf{w}_t)\|_2^2 \right) \\
&\leq \rho^T F_1 + \frac{\alpha n L_{2,\infty}^2}{2} \left(12\rho^{T-1} \alpha^2 n^2 \sigma^2 + \frac{28\rho \alpha^2 (\varsigma + \sigma)^2 \tilde{A}^2}{(1-\rho)m^2} \right) \\
&\leq \rho^T F_1 + \rho^{T-1} 6\alpha^3 n^3 L_{2,\infty}^2 \sigma^2 + \frac{28\rho \alpha^3 n L_{2,\infty}^2 (\varsigma + \sigma)^2 \tilde{A}^2}{\alpha n \mu m^2} \\
&\leq \rho^T F_1 + \rho^T 7\alpha^3 n^3 L_{2,\infty}^2 \sigma^2 + \frac{28\rho \alpha^3 n L_{2,\infty}^2 (\varsigma + \sigma)^2 \tilde{A}^2}{\alpha n \mu m^2} \\
&\leq \rho^T (F_1 + \sigma^2/L_{2,\infty}) + \frac{28\alpha^2 L_{2,\infty}^2 (\varsigma + \sigma)^2 \tilde{A}^2}{\mu m^2} \\
&\leq (F_1 + \sigma^2/L_{2,\infty}) \exp(-T\alpha n \mu/2) + \frac{28\alpha^2 L_{2,\infty}^2 (\varsigma + \sigma)^2 \tilde{A}^2}{\mu m^2},
\end{aligned}$$

where we have further constrained $\alpha \leq \frac{2}{9n\mu}$ so that $\rho \leq 9/8$ in the forth inequality and $\alpha \leq \frac{1}{7^{1/3} n L_{2,\infty}}$ in the fifth inequality. By setting the derivative w.r.t α of the RHS to 0, the minimizer α under the constraint that $0 < \alpha \leq \min \left\{ \frac{2}{9n\mu}, \frac{1}{16 \max\{L_\infty, L_{2,\infty}\}(2n + \tilde{A}/m)} \right\}$ (required by the lemmas) is:

$$\alpha = \frac{2}{T n \mu} W_0(T^2 m^2 n^2 C_3),$$

as long as

$$\begin{aligned}
T &\geq 1 + \frac{2}{n\mu} \max\{(9/2)n\mu, 16 \max\{L_\infty, L_{2,\infty}\}(2n + \tilde{A}/m) W_0(T^2 m^2 n^2 C_3)\} \\
&= 10 + \frac{1}{\mu} 32 \max\{L_\infty, L_{2,\infty}\}(2 + \tilde{A}/(mn)) W_0(T^2 m^2 n^2 C_3),
\end{aligned}$$

where $C_3 = \frac{(F_1 + \sigma^2/L_{2,\infty})\mu^2}{224L_{2,\infty}^2(\varsigma + \sigma)^2 \tilde{A}^2}$. What he did here was to set T just large enough so that the minimizer α is the same with or without the constraint. Denote $\tilde{W} = W_0(T^2 m^2 n^2 C_3) = \tilde{O}(1)$, we get:

$$\begin{aligned}
F_{T+1} &\leq \frac{(F_1 + \sigma^2/L_{2,\infty})\tilde{W}}{T^2 m^2 n^2 C_3} + \frac{112L_{2,\infty}^2 (\varsigma + \sigma)^2 \tilde{A}^2 \tilde{W}^2}{T^2 m^2 n^2 \mu^3} \\
&\leq \frac{1}{T^2 m^2 n^2} \left(\frac{(F_1 + \sigma^2/L_{2,\infty})\tilde{W}}{\tilde{C}_3} + \frac{112L_{2,\infty}^2 (\varsigma + \sigma)^2 \tilde{A}^2 \tilde{W}^2}{\mu^3} \right),
\end{aligned}$$

which shows the convergence rate in the P.L. case is $\tilde{O}((mnT)^{-2})$. □

D Experiment Details

Here we provide more extensive details on our empirical results. This includes background information on our experimental setup in the main paper (Appendix D.1), an additional simulation experiment on pre-training and fine-tuning Tiny GPT-2 (Appendix D.2), and an additional simulation experiment that investigates CD-GraB with different learning rates (Appendix D.3)

D.1 Additional details on setup for main paper experiments

D.1.1 Distributed experiments

We provide additional details on the experiments shown in Figure 3.

Hardware and software. We use a single machine with 128 GiB memory, 1 CPU, and 4 Nvidia GeForce 2080ti GPUs for the HMDA mortgage application, M4, and WikiText-2 tasks. We first discard the remainder $N \bmod B$, and then randomly partition n to each worker. Our experiments are all implemented with the PyTorch library. We release our code suite at [REDACTED].

Datasets and models.

- **Logistic regression on mortgage application (NY 2017 subset):** The US Home Mortgage Disclosure Act (HMDA) makes available US national data regarding mortgage applications, which has recently been packaged up for easy ML research use [7]. We use the binary classification version of the task, which classifies features as either “grant loan” or “deny loan,” for the New York (NY) 2017 subset of the dataset, which includes 244107 examples with 18 features. We model this problem using logistic regression, for which we first perform a random 80/20 train/test split on the raw dataset, and then we discard $N \bmod B$ (B is the aggregated minibatch size) examples to ensure that each worker receives exactly n examples. We use 1 worker per GPU, and in total we have $m = 4$ workers, and use NCCL [33] as the distributed communication backend; $m = 4$, $n = 48816$, $d = 18$, $B = 16$. We report test accuracy as our evaluation metric.
- **LSTM on WikiText-2:** We follow the settings in Lu et al. [24] and train a 2-layer LSTM with an embedding size of 32 and dropout set to 0. We use backpropagation through time, for which we set the sequence length to 35. We also adopt the word-vector-classifier-weight-sharing strategy inspired by Inan et al. [19]. WikiText-2 [43] has 600 articles in the train set, with more than 2M tokens and 30K vocabulary; the validation and test sets each have 60 articles. We adapt our training script from PyTorch’s official Word Language Modeling Github repository. We use 4 workers in total, with each GPU hosting 1 worker, and use NCCL as the distributed communication backend; $m = 4$, $n = 3728$, $d = 1081760$, $B = 16$. We report test perplexity as the evaluation metric, and we follow the HuggingFace’s approach of computing perplexity as the exponentiated average negative log-likelihood of a sequence¹².
- **Autoregressive MLP on M4 Weekly Dataset:** We build a 3-layer autoregressive MLP with a hidden dimension of 64. We set input sequence length to be 20 and the output sequence length to be 6. M4 is a time series dataset composed of 100,000 time series for yearly, quarterly, monthly, weekly, daily and hourly data [25], which is drawn from a random sample of ForeDeCk database [42]. We use the weekly data in our experiment. We use 32 workers, where each of the 4 GPUs hosts 8 process workers. We use GLOO as the distributed communication backend. $m = 32$, $n = 3355$, $d = 5569$, $B = 32$. We report test symmetric mean absolute percentage error (SMAPE) as the evaluation metric. We follow the formula of SMAPE in [25] as follows:

$$\text{SMAPE} \triangleq \frac{2}{h} \sum_{t=n+1}^{n+h} \frac{|Y_t - \hat{Y}_t|}{|Y_t| + |\hat{Y}_t|} * 100\%$$

where Y_t is the reference time series value at timestep t , \hat{Y}_t is the forecast time series value at timestep t , and h is the forecasting horizon and n is the number of datapoints.

Hyperparameter optimization. For all tasks, we tune the learning rate α for D-RR first, and then use the selected learning rate for CD-GraB. Therefore, an performance improvement here implies we would have in-place

¹²<https://huggingface.co/docs/transformers/perplexity>

substitution benefits via switching from D-RR to CD-GraB with identical learning rate and experiment setups. We use SGD with momentum as the optimizer for all tasks. The hyperparameters for each task are as follows:

- **Logistic regression on mortgage application (NY 2017 subset):** $\alpha = 1e-2 \in \{1e-2, 1e-3, 1e-4\}$, momentum: 0.9, weight decay: 0, B : 16.
- **LSTM on WikiText-2:** $\alpha = 5 \in \{5, 10\}$ and decays by 0.1 per 10 epochs, momentum: 0.9, weight decay: 0, B : 32.
- **Autoregressive MLP on Weekly M4 Dataset** $\alpha = 1e-2 \in \{1e-2, 1e-3, 1e-4\}$, momentum: 0.9, weight decay: 0, B : 16.

D.1.2 Simulated ablation study using LeNet on CIFAR-10

In the experiment shown on Figure 4, we select the same learning rate, momentum, and weight decay as the LeNet experiment in Lu et al. [24]. We use 3 different random seeds to control 3 different initialization and the randomness in random reshuffling. The aggregated minibatch size B is 64 for all runs. We implement this ablation study by using 1 GPU with up to $m = 64$ workers (processes). As above, we discard $N \bmod B$ examples and partition the remaining examples evenly on each worker.

$\alpha = 1e-3 \in \{1e-2, 5e-3, 1e-3, 5e-4, 1e-4\}$, momentum: 0.9, weight decay: $1e-4$, B : 64.

We do not implement this via distributed environment due to the fact that we do not have access to 64 GPUs, but expect the simulation results to be a good reflection of the results we would obtain in a multi-GPU setting.

Parallel herding bound. We further investigate the empirical parallel herding bounds (8) for the LeNet experiment for the different ordering methods. We plot the results in Figure 7. We observe that as the number of workers increases, the empirical parallel herding bounds of both **ID-GraB (Bal)** and **ID-GraB (PairBal)** also increase, and eventually exhibit little difference with D-RR. CD-GraB, in contrast, exhibits a consistently lower bound.

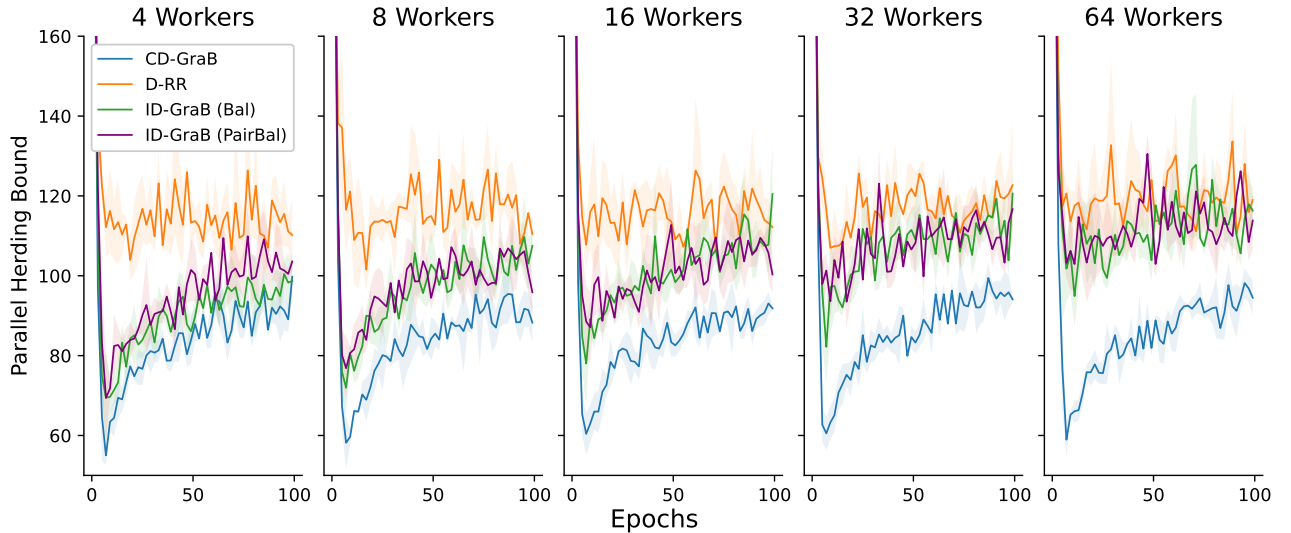


Figure 7: Empirical parallel herding bounds of gradients for each algorithm in LeNet experiment. We plot the mean as the curve and standard deviation across 3 random seeds.

For comparison, we also run a simulation experiment on synthetic data to investigate the behavior of the parallel herding bound. We include these below, in Figure 8.

We randomly initialize 1 million random vectors $z_{i,j}$ from a uniform distribution between 0 and 1 with 16 dimensions as $z_{i,j} \sim \text{Unif}(0, 1)^{16}$, and then we zero-center this set of 1 million vectors and normalize them to all have L_2 norm as 1. We then evenly partition this set of 1 million random vectors to $\{5, 10, 20, 50, 100\}$ workers and run each example ordering algorithm.

In Figure 8, we run CD-GraB, D-RR, **ID-GraB (Bal)**, **ID-GraB (PairBal)** on these random vectors, and compute the parallel herding bounds (8). From left to right in Figure 8, we observe that as the number of

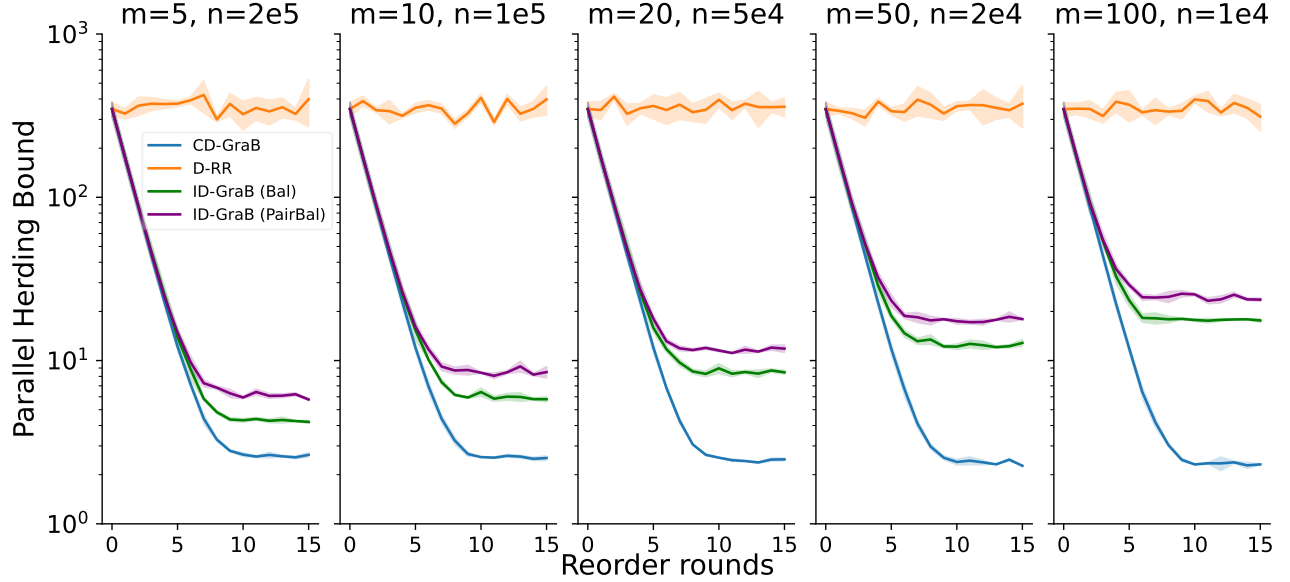


Figure 8: Parallel herding bounds for different example ordering algorithms on $N=1$ million random vectors. We use 3 random seeds, plot the mean and standard deviation across each random seed as the shaded area.

workers m increases, the parallel herding bound of **ID-GraB (Bal)**, **ID-GraB (PairBal)** becomes larger. This shows the importance of coordination when we have a large number of workers.

These results for random vectors cohere with our above results for LeNet on CIFAR-10.

D.2 An additional simulation experiment: pre-training and fine-tuning Tiny GPT-2

We perform an end-to-end simulation experiment involving pre-training and fine-tuning Tiny GPT-2 on WikiText-103, which we document below.

D.2.1 Pre-training

We adapt the training script from the HuggingFace’s PyTorch casual language modeling codes to train the GPT-2 architecture [35]. We set the maximum sequence length to 128 and token and positional embedding dimension to 128; use 2 hidden layers in the transformer encoder and 2 attention heads; and disable dropout. This model configuration corresponds to the following Python code snippet:

```

1 from transformers import GPT2Config, GPT2LMHeadModel, GPT2Tokenizer
2
3 tokenizer = GPT2Tokenizer.from_pretrained('gpt2')
4 config = GPT2Config.from_pretrained('gpt2')
5 config.n_embd = 128
6 config.n_ctx = 128
7 config.n_layer = 2
8 config.n_head = 2
9 config.n_positions = 128
10 config.summary_first_dropout = 0
11 config.attn_pdrop = 0
12 config.resid_pdrop = 0
13 model = GPT2LMHeadModel(config)

```

We train our Tiny GPT-2 model from scratch on WikiText-103 [43]. WikiText-103 is a standard language modeling benchmark that has 28,475 articles in the train set, and 60 for both the validation and test sets, with more than 100M tokens and 267K vocabulary inside the train set. We use the original GPT-2 tokenizer, and use maximum sequence length 128. We note that this is much smaller than the default maximum sequence length for GPT-2, which is 1024, which was too large to use given our computational budget. Nevertheless, 128 is still a reasonable sequence length for the initial phrase of pre-training; BERT uses a sequence length of 128 for the first

90% of pre-training steps to speedup the experiment [9]. We tune the learning rate for D-RR with the grid $\{5e-3, 1e-3, 5e-4, 1e-4\}$ (the final learning rate is $5e-4$), and use AdamW optimizer [21]. We use 3 random seeds. Before the training, we simulate 64 workers, and similarly divide the training dataset evenly across them by discarding $N \bmod B$ examples. Our hyperparameter optimization space is listed below:

Pretraining Hyperparameters. $\alpha = 5e-4 \in \{5e-3, 1e-3, 5e-4, 1e-4\}$, weight decay: $1e-4$, B : 64.

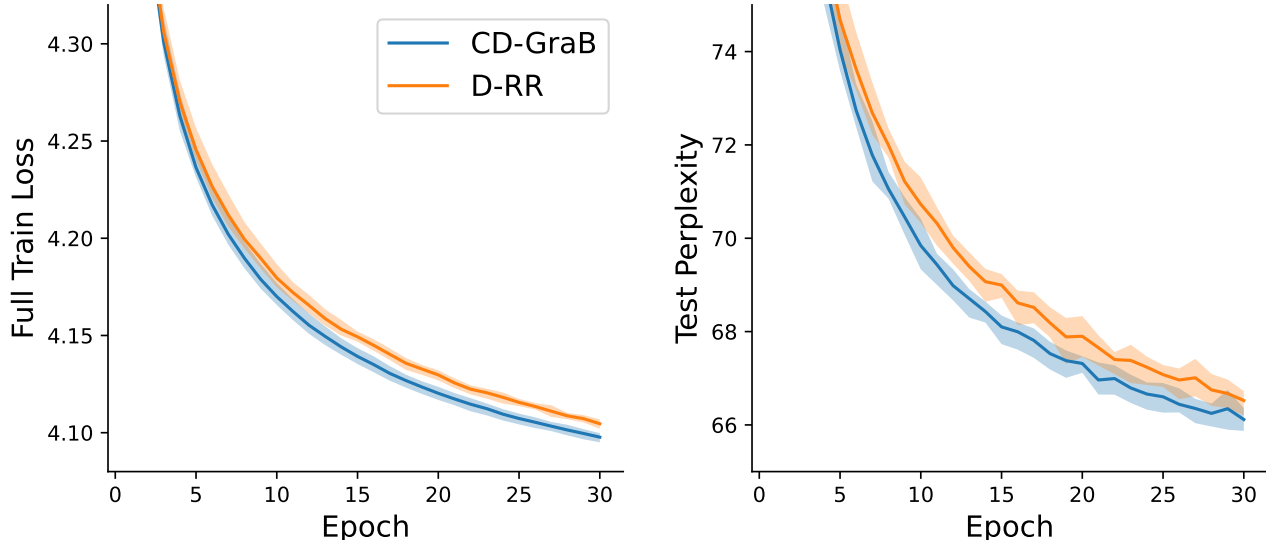


Figure 9: Pre-training Tiny GPT-2 on WikiText-103 from scratch: Convergence for CD-GraB and D-RR with $m = 64$ workers. The aggregated minibatch size per update is 64. We use 3 random seeds, and plot the mean and standard deviation.

We document convergence for pre-training in Figure 9, and use test perplexity as our evaluation metric.

D.2.2 Fine-tuning

We then finetune the pre-trained Tiny GPT-2 model on downstream tasks. For each task, we load the pre-trained foundation model weights obtained at the end of 30 epochs of each example ordering algorithm after pretraining, and use the same example ordering algorithm to perform supervised fine-tuning. We focus on the largest 4 GLUE tasks [44]: MNLI, QQP, QNLI, and SST2. We tune the learning rate for D-RR with the AdamW optimizer, and for each run we report the best validation accuracy. We then take an average results of each run and summarize them in Table 1. Our training script is adapted from the HuggingFace’s PyTorch GLUE finetuning example code.

Finetuning Hyperparameters

- **MNLI** $\alpha = 5e-4 \in \{5e-3, 1e-3, 5e-4, 1e-4\}$, Weight decay: $1e-4$, B : 32, epochs: 10, linear learning rate scheduler
- **QQP** $\alpha = 5e-4 \in \{5e-3, 1e-3, 5e-4, 1e-4\}$, Weight decay: $1e-4$, B : 32, epochs: 10, linear learning rate scheduler
- **QNLI** $\alpha = 5e-4 \in \{5e-3, 1e-3, 5e-4, 1e-4\}$, Weight decay: $1e-4$, B : 32, epochs: 10, linear learning rate scheduler
- **SST2** $\alpha = 5e-4 \in \{5e-3, 1e-3, 5e-4, 1e-4\}$, Weight decay: $1e-4$, B : 32, epochs: 10, linear learning rate scheduler

We include these fine-tuning results in part to support our claim in Section 6 that CD-GraB exhibits its benefits more clearly when there are more training epochs. Our pre-training results suggest that CD-GraB would confer benefits to pre-training large models over multiple epochs; however, CD-GraB will not necessarily be useful for short runs of fine-tuning (as indicated in Table 1, for which the results for both ordering algorithms are effectively identical).

	MNLI (Matched)	MNLI (Mismatched)	QQP	QNLI	SST2
CD-GraB	65.91 \pm 0.46 %	64.36 \pm 2.03 %	82.25 \pm 0.21 %	62.11 \pm 0.70 %	82.65 \pm 0.39 %
D-RR	65.42 \pm 0.36 %	63.93 \pm 1.63 %	81.74 \pm 0.33 %	61.87 \pm 0.67 %	82.68 \pm 0.57 %

Table 1: GLUE fine-tuning datasets: Validation accuracy of CD-GraB in comparison to D-RR, reporting mean and standard deviation of best results for each run. There are 3 runs for each example ordering algorithm.

D.3 Ablation simulation study: The impact of learning rate α

In the experiment shown on Figure 10, we select the same momentum and weight decay as the LeNet experiment for 3 random seeds as in Appendix D.1.2. The aggregated minibatch size is still 64 for all runs, and we use 64 workers.

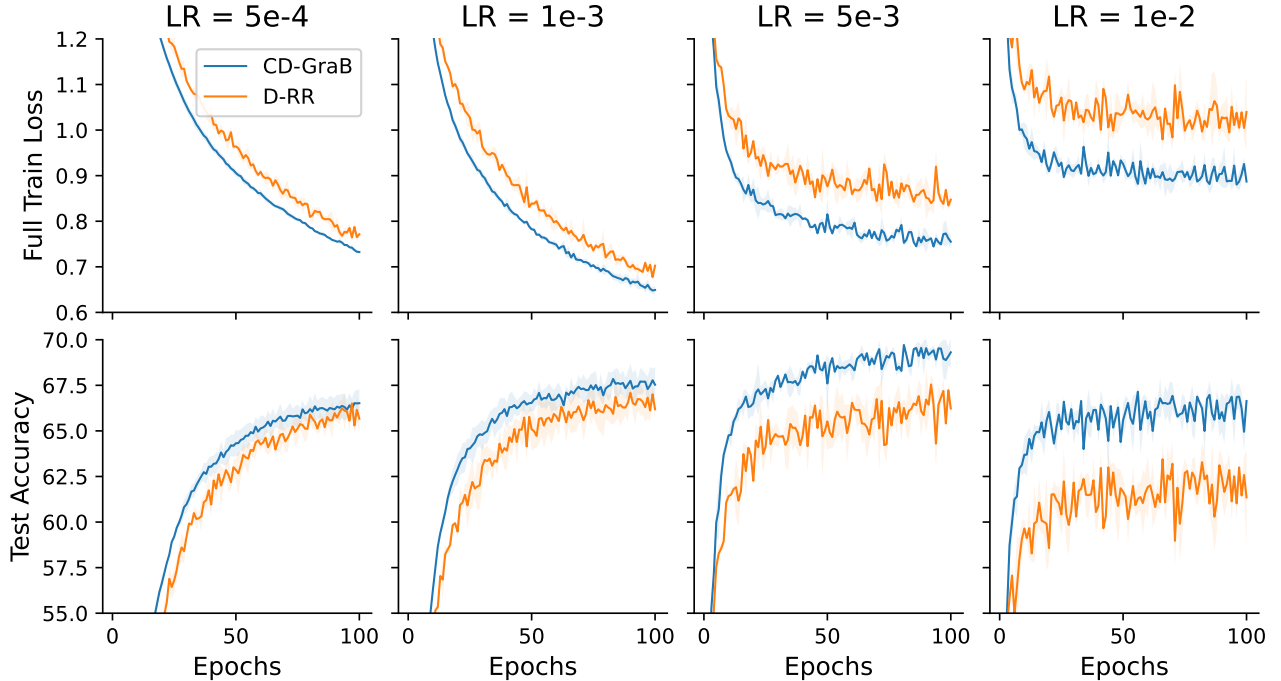


Figure 10: Convergence for CD-GraB, D-RR training LeNet on CIFAR-10, with $m = 64$ workers. The aggregated minibatch size per update is 64. We use 3 random seeds, and plot the mean values across random seeds as the curve, the standard deviation as the shaded area.

We find that when we increase the learning rate from 1e-3 to 1e-2, CD-GraB still maintains relatively better performance than D-RR. The best learning rate for D-RR is 1e-3, in terms of achieving the best test accuracy. We did not tune the learning rate for CD-GraB, and we expect that it is possible to use a higher learning rate and still maintain better empirical performance than D-RR and even faster convergence. We defer such empirical investigations to future work. Altogether, these preliminary empirical results confirm that it is possible to use higher learning rate for CD-GraB, given that online PairBalance does not need to use a stale mean (Section 3.2), which would make larger learning rates perform poorly.